NuRD chromatin remodeling is required to repair exogenous DSBs in the *Caenorhabditis elegans* germline

Deepshikha Ananthaswamy[1], Kelin Funes[1†], Thiago Borges[1†], Scott Roques[1], Nina Fassnacht[2], Sereen El Jamal[2], Paula M. Checchi[2], Teresa Wei-sy Lee[1]*

[1] Department of Biological Sciences, University of Massachusetts Lowell, 198 Riverside Dr. Lowell MA, 01854

[2] Department of Biology, Marist College, 3399 North Road, Poughkeepsie, NY 12601

† contributed equally

* for correspondence, teresa_lee@uml.edu

Running title: NuRD remodeling repairs exogenous DSBs

Keywords: DNA repair, NuRD (nucleosome remodeling and deacetylase complex), LET-418/CHD4, FCD-2/FANCD2, germline

ABSTRACT

Organisms rely on coordinated networks of DNA repair pathways to protect genomes against toxic double-strand breaks (DSBs), particularly in germ cells. All repair mechanisms must successfully negotiate the local chromatin environment in order to access DNA. For example, nucleosomes can be repositioned by the highly conserved Nucleosome Remodeling and Deacetylase (NuRD) complex. In *Caenorhabditis elegans*, NuRD functions in the germline to repair DSBs – the loss of NuRD's ATPase subunit, LET-418/CHD4, prevents DSB resolution and therefore reduces fertility. In this study, we challenge germlines with exogenous DNA damage to better understand NuRD's role in repairing DSBs. We find that *let-418* mutants are sensitive to cisplatin and hydroxyurea: exposure to either mutagen impedes DSB repair, generates aneuploid oocytes, and reduces fertility and embryonic survival. These defects resemble those seen when the Fanconi anemia (FA) DNA repair pathway is compromised, and we find that LET-418's activity is epistatic to that of the FA component FCD-2/FANCD2. We propose a model in which NuRD is recruited to the site of DNA lesions to remodel chromatin and allow access for FA pathway components. Together, these results implicate NuRD in the repair of both endogenous DSBs and exogenous DNA lesions to preserve genome integrity in developing germ cells.

ARTICLE SUMMARY

Preserving genome integrity in germ cells is critical for the survival of individuals and species. Our previous work shows that nucleosome remodeling plays an important role in repairing meiotic DNA damage. Here, we further challenge genomes with toxic DNA damaging agents to test the requirement for remodeling in the germline. We find that DNA damage accumulates in the absence of remodeling, which drastically reduces oocyte quality, and also show that the requirement for remodeling is epistatic to the Fanconi anemia DNA repair pathway. These findings demonstrate that local chromatin environments must be remodeled in response to DNA damage to maintain oocyte quality.

INTRODUCTION

DNA damage poses a danger to all cells, but if left unrepaired in germ cells, it is deleterious for organismal survival. During meiosis, any DNA lesion that persists until chromosome segregation will generate an aneuploid gamete, which in turn causes infertility or embryonic lethality (Ceccaldi et al., 2016; Kim et al., 2016). The evolutionary pressure to protect genomes for future generations has generated multiple distinct, but overlapping, DNA repair pathways. These pathways handle both endogenous programmed double-strand breaks (DSBs) required for crossover recombination, along with any exogenous DNA damage incurred in the germline (Chapman et al., 2012; Gartner and Engebrecht, 2022; Keeney, 2007). Studies in organisms ranging from budding yeast to mammals have identified strong conservation among these repair pathways, which include error-free mechanisms like homologous recombination and error-prone mechanisms like non-homologous end joining (De Massy, 2013; Stinson and Loparo, 2021, 2021; Wilson et al., 1997). For example, the Fanconi anemia (FA) pathway is activated when replication forks collide with DNA interstrand crosslinks, which are one of the most toxic DNA lesions (Gartner and Engebrecht, 2022). Components of the FA pathway coordinate the excision of the crosslink and conversion to DSBs, which can then be resolved by the meiotic homologous recombination pathway (Adamo et al., 2010; Lachaud et al., 2016; Raghunandan et al., 2015; Schlacher et al., 2012). Defects in the FA pathway are linked to an elevated risk of cancer and cause chromosomal instability or meiotic catastrophe, hallmarks of the rare congenital disorder of Fanconi anemia (Auerbach, 2009, 1993; Ceccaldi et al., 2016; De Winter and Joenje, 2009; Nalepa and Clapp, 2018; Tischkowitz et al., 2003, 2004).

In eukaryotes, DNA repair must always happen in the context of chromatin, where DNA is wrapped around histone octamers to form nucleosomes (Allis and Jenuwein, 2016). Nucleosomes act as obstacles that control access to DNA, and therefore their spacing is regulated by nucleosome remodeling complexes (Becker and Workman, 2013). The highly conserved remodeling complex, Nucleosome remodeling and deacetylase (NuRD), includes ATPase remodelers from the chromodomain helicase DNA binding (CHD) family (Basta and Rauchman, 2015; Kehle, 1998; Tong et al., 1998; Wade et al., 1998; Woodage et al., 1997; Xue et al., 1998). In addition to CHD remodeling subunits, NuRD also consists of the histone deacetylases HDAC1/2, histone demethylase LSD1/KDM1A, and other components that allow NuRD to bind modified histones, methyl CpG, and other proteins (Basta and Rauchman, 2015; Wang et al., 2009; Whyte et al., 2012). Initially, NuRD's primary role was thought to be transcriptional repression; but studies have since identified a more nuanced involvement in gene expression, along with other biological functions like DNA repair (Basta and Rauchman, 2015). The

58 nematode *Caenorhabditis elegans* has two catalytic CHD paralogs associated with the core NuRD
59 complex: CHD-3 (also known as Mi-2α or CHD3 in mammals) and LET-418 (Mi-2β or CHD4) (Passannante
60 et al., 2010; von Zelewsky et al., 2000). Mutations in either the *chd-3* or the *let-418* genes severely
61 reduce fertility due to high levels of persistent meiotic DSBs (McMurchy et al., 2017; Turcotte et al.,
62 2018).
63 These studies highlight the importance of NuRD's role in the germline for proper DNA repair –
64 the loss of NuRD activity appears to shunt DSBs from error-free repair towards error-prone pathways
65 like NHEJ. The genomic instability of *chd-3* or *let-418* mutants resembles those seen in mutants
66 defective for the FA pathway (Rageul and Kim, 2020; Tsui and Crismani, 2019; Turcotte et al., 2018). One
67 hallmark of mutations in FA components is an increased sensitivity to mutagens like cisplatin, which
68 induces DNA interstrand crosslinks, or hydroxyurea, which stalls replication forks (Bailly and Gartner,
69 2011; Datta and Brosh Jr., 2019; Youds et al., 2009). Both of these lesions can generate DSBs if left
70 unrepaired, which activate the S-phase checkpoint and subsequently delays cell cycle progression
71 (Kessler and Yanowitz, 2014; Kim and Colaiácovo, 2015). Resolution of interstrand crosslinks by the FA
72 pathway involves recognition and binding by the core FA complex, which then recruits FANCD2 to
73 chromatin by mono-ubiquitination (Nakanishi et al., 2005; Niraj et al., 2019). Once at the DNA lesion,
74 FANCD2 orchestrates the repair of the lesion by converting it to DSBs, which are then resolved by
75 homologous recombination (Ceccaldi et al., 2016; Niraj et al., 2019).
76 NuRD is required for repairing DNA lesions in germ cells (McMurchy et al., 2017; Turcotte et al.,
77 2018), but it is not clear how or whether nucleosome remodeling interacts with repair processes like the
78 FA pathway. Here, we challenge the germline by inducing exogenous DNA damage to investigate the
79 relationship between the FA pathway and NuRD's catalytic component, LET-418/CHD4. *C. elegans* has
80 homologs for many core FA components, including FCD-2/FANCD2 (Kim et al., 2018; Lee et al., 2010).
81 One advantage of using *C. elegans* for this study is the germline's spatiotemporal organization, which
82 allows us to easily follow the effects of mutagen exposure at multiple downstream stages during
83 oogenesis (Jaramillo-Lambert et al., 2007; Kessler and Yanowitz, 2014). We show that LET-418 activity is
84 epistatic to FCD-2 and is necessary to repair germline DSBs and preserve fertility. These results support a
85 model where NuRD generates a permissive local chromatin environment at the site of DNA damage to
86 allow access to DSB repair machinery and therefore preserve gamete quality in the face of genotoxic
87 stress.
88
89 **METHODS**

90 Strains and husbandry: All strains were cultured using standard methods (Brenner, 1974) at 20°C on 6-
91 cm NGM agar plates spotted with OP50 *E. coli* grown overnight at 37°C in Luria Broth (LB). Gene and
92 sequence information was downloaded from WormBase (Davis et al., 2022). The *syb6818* allele is a
93 deletion of LET-418's ATPase domain and removes amino acids 590-1114. The *syb6708* allele is a
94 deletion of LET-418's PHD finger domain and removes amino acids 256-365. Both domains were
95 identified using an NCBI structure prediction and based on homology with human CHD4 (Farnung et al.,
96 2020; Sayers et al., 2022). TER6 is a homozygous sterile strain, and was maintained over an *nT1* balancer
97 chromosome by picking GFP-positive heterozygotes. The following strains were obtained from the
98 *Caenorhabditis* Genetics Center or were generated by SunyBiotech (*syb* alleles, which were backcrossed
99 five times to N2):

100 - N2: wild-type (Bristol isolate)
101 - MT14390: *let-418 (n3536) V*
102 - NB105: *fcd-2 (tm1298) IV*
103 - TG1660: *xpf-1 (tm2842) II*
104 - TER14: *fcd-2 (tm1298) IV; let-418 (n3536) V*
105 - TER6: *let-418 (syb6818)/nT1 [qIs51] IV:V*
106 - TER10: *let-418 (syb6708) V*

107

108 Mutagen exposure: All exposure assays were performed on hermaphrodites cultured at 20°C on 3-cm
109 NGM agar plates. Plates were first spotted with OP50 *E. coli*, then treated by spreading 250 µL of either
110 400 µM cisplatin (Sigma Aldrich) or 10 mM hydroxyurea (Thermo Scientific) onto agar at least 12 hours
111 prior to experiment. Synchronized young adult hermaphrodites (12 hours post-L4 larval stage) were
112 placed on mutagen plates for 24 hours, then moved to regular NGM plates to recover before assessing
113 nuclei in the appropriate meiotic stage; the timing for each assay is described below (Jaramillo-Lambert
114 et al., 2007; Kessler and Yanowitz, 2014).

115

116 Immunofluorescence and image processing: To assess RAD-51 foci in the mitotic region after mitotic
117 exposure, exposed and control hermaphrodites were allowed to recover on NGM plates for four hours
118 before dissection to produce better gonad extrusion. To assess RAD-51 foci in pachytene after mitotic
119 exposure, hermaphrodites were allowed to recover for 30-40 hours, allowing nuclei to progress to mid-
120 to late-pachytene. Gonad dissection, fixation, and immunostaining were performed as previously
121 described (Ananthaswamy et al., 2022). In brief, gonads were dissected using 25-gauge syringe needles,

122 fixed in 0.8% paraformaldehyde (Electron Microscopy Services) for five minutes at room temperature,
123 subjected to freeze crack, and dehydrated in 100% methanol for one minute at -20°C. Slides were
124 washed three times with PBS + 0.1% Tween-20 (Thermo Scientific) prior to overnight incubation at room
125 temperature with primary antibody. Slides were washed three times before incubation with secondary
126 antibody for four hours at room temperature. Samples were mounted in VectaShield (Vector
127 Laboratories) with 2 µg/ml DAPI (Thermo Life) before sealing with nail polish. Antibodies used were
128 rabbit anti-RAD-51 at 1:5000 (a gift from Diana Libuda (Kurhanewicz et al., 2020)) and donkey anti-rabbit
129 AlexaFluor594 at 1:400 (Invitrogen).
130 Immunofluorescence images were collected at 63x as Z-stacks with 0.25 µm intervals using a
131 Zeiss Axio Imager M2 microscope with Zen 3.8 software (Zeiss). All representative images shown are
132 max projections after processing in FIJI software (Schindelin et al., 2012). Unprocessed Z-stacks were
133 used to quantify RAD-51 foci. Three biological replicates were performed, with three to five gonads
134 imaged per condition in each replicate. Only one gonad arm was analyzed from each hermaphrodite. In
135 the mitotic region, all nuclei were scored for RAD-51 foci. In pachytene, only nuclei in the top row were
136 scored for RAD-51 foci; pachytene regions were determined by counting the number of rows after the
137 transition zone and before diplotene, and dividing into equal thirds. Some nuclei had a distinctive
138 apoptotic appearance with collapsed, DAPI-bright chromosomes and an excess of RAD-51 staining; these
139 were included in the total nuclei number, but not scored for RAD-51 foci. All statistical analyses were
140 performed in Prism 8 (GraphPad), with *P*-values determined using a Kruskal-Wallis non-parametric test
141 after a Dunn's post-hoc test used to account for pairwise comparisons.
142
143 Analysis of diakinesis DAPI bodies: Following exposure to cisplatin or hydroxyurea, hermaphrodites were
144 allowed to recover for 60 hours, allowing mitotic oocyte nuclei to progress through meiosis to diakinesis.
145 Gonads were dissected as previously described (Ananthaswamy et al., 2022) with the following
146 modifications: the primary and secondary antibody incubation steps were skipped, and slides were
147 washed at least three times in PBS + 0.1% Tween-20 (Thermo Scientific) before mounting in SlowFade
148 Diamond (Molecular Probes) with 2 µg/ml DAPI (Thermo Life). Images were collected at 63x as Z-stacks
149 with 0.25 µm intervals captured on Zeiss Axio Imager M2 using Zen 3.8 software (Zeiss). All
150 representative images shown are max projections after processing in FIJI (Schindelin et al., 2012).
151 Unprocessed z-stacks were used to quantify DAPI-stained bodies in the -1 to the -4 oocyte from the
152 spermatheca. Three biological replicates were performed, with each condition consisting of a minimum

153 of 100 nuclei from at least 27 hermaphrodites. All statistical analyses were performed in Prism 10
154 (GraphPad), with p-values determined using a Fisher's exact test on a 2x5 contingency table.
155
156 Embryonic survival – 4-hr laying period: After exposure to cisplatin, hydroxyurea, or nitrogen mustard,
157 hermaphrodites were allowed to recover on NGM plates for 60 hours, allowing mitotic oocyte nuclei to
158 progress through the gonad and be laid as fertilized embryos. Exposed mothers were then moved onto
159 freshly spotted 3-cm NGM plates (five to ten mothers per plate) and allowed to lay for four hours before
160 being removed from plates. The number of embryos per plate was immediately recorded after removal
161 of mothers, and were scored as fertilized, unfertilized, or dead. Hatched progeny were counted as adults
162 three days later. Percent survival was calculated by dividing the number of hatched progeny by the
163 number of embryos, multiplied by 100. Each condition consists of progeny from 125-150 mothers,
164 collected over three biological replicates. All statistical analyses were performed in Prism 8 (GraphPad),
165 with p-values determined from a one-way ANOVA after a Šídák correction used to account for multiple
166 comparisons.
167
168 Embryonic survival – entire brood: Individual hermaphrodites were isolated on separate plates as L4
169 larvae and transferred every 12 hours until the end of their fertile period (usually 5-6 days). Embryos
170 and unfertilized eggs were counted every 12 hours immediately after transfer of the mother. Total
171 brood was calculated for each mother as all embryos laid during the fertile period. Hatched progeny
172 were then counted two to three days later (when they were L4s or young adults). Percent survival was
173 calculated by dividing the number of hatched progeny by the number of embryos laid and multiplied by
174 100. Each biological replicate includes the broods of five mothers scored for each genotype (i.e. five
175 technical replicates). The following biological replicates were performed: seven of N2; six of *let-418*
176 *(n3536)*; four of *let-418 (syb6818)*; and four of *let-418 (syb6708)*. Broods were censored from analysis if
177 the mother died of unnatural causes before the end of their fertile period (usually from vulva rupture or
178 crawling off the agar). All statistical analyses were performed in Prism 8 (GraphPad), with p-values
179 determined from a one-way ANOVA after a Šídák correction used to account for multiple comparisons.
180
181 **RESULTS**
182 LET-418 activity is required to repair mitotic DNA lesions in mitosis and meiosis.
183 Mutants lacking both NuRD paralogs (CHD3 and CHD4) have severely compromised fertility,
184 which makes downstream analyses difficult (Turcotte et al., 2018). Therefore, we focused only on the

185 impact of LET-418/CHD4, reasoning that it plays a larger role in repairing germline DSBs because its loss
186 causes more meiotic defects than that of CHD-3 (Turcotte et al., 2018). A previous study noted that at
187 pachytene entry, *let-418* mutants have more DSBs than wild-type (Turcotte et al., 2018), leading us to
188 wonder whether these DSBs represent unrepaired DNA damage acquired during replication. Because
189 DSBs are rare in mitotic nuclei, we used cisplatin and hydroxyurea to generate exogenous DNA damage
190 and further stress the DNA repair process. We examined *let-418 (n3536)* missense hypomorphic
191 mutants and *fcd-2 (tm1298)* deletion mutants, which lack the FA pathway component FCD-2/FANCD2.
192 We capitalized on the fact that the *C. elegans* germline is organized in a spatiotemporal manner, with
193 nuclei undergoing mitosis at the distal tip and moving proximally as they proceed through meiosis. The
194 timing of how nuclei progress through mitotic replication, meiosis, oocyte maturation, and fertilization
195 has been extensively characterized (Jaramillo-Lambert et al., 2007; Kessler and Yanowitz, 2014). We
196 therefore estimated the timing after exposure to capture the impact of DNA damage incurred during
197 mitosis.
198 Mitotic zone DSBs were assessed using an antibody for the RecA recombinase RAD-51, a
199 common cytological marker for DSBs (Alpi et al., 2003; Colaiácovo et al., 2003; Kurhanewicz et al., 2020).
200 Hermaphrodites were cultured on either cisplatin or hydroxyurea for twenty hours, allowed to recover
201 for four hours, and dissected for immunofluorescence (Jaramillo-Lambert et al., 2007; Kessler and
202 Yanowitz, 2014). Consistent with prior reports, unexposed wild-type animals accumulated few RAD-51
203 foci in the mitotic zone (Fig. 1A, C, Fig. 2A, C, and Table S1) (Alpi et al., 2003; Turcotte et al., 2018), which
204 was also true for all mutants examined, with foci in less than 8% of nuclei. Unexposed *let-418* single
205 mutants had a modest but significant increase in foci compared to wild-type animals ($P < 0.0001$,
206 Kruskal-Wallis test), but neither *fcd-2* single mutants nor *fcd-2; let-418* double mutants had more foci
207 than wild-type (Fig. 1A, $P > 0.08$ for both comparisons, Kruskal-Wallis test). Unexposed *fcd-2; let-418*
208 double mutants were not more affected than either single mutant ($P > 0.8$ for both comparisons,
209 Kruskal-Wallis test). We note that, although the average number of foci did not vary much between
210 genotypes, we occasionally observed nuclei with two or three foci in *let-418* single mutants (0.8% of
211 nuclei) and *fcd-2; let-418* double mutants (0.7%), which were rarely seen in wild-type germlines (0.2%)
212 (Fig. 1A and Table S1).
213 As expected, exposure to 400 µM cisplatin increased the number of RAD-51 foci across all
214 genotypes compared to unexposed controls (Fig. 1B, D and Table S1). This dose was chosen based on a
215 dose curve showing that 400 µM drastically reduced embryonic survival in both wild-type and mutant
216 populations (Fig. S1 and Table S6). Wild-type populations exposed to cisplatin accumulated over five

217 times more foci than their unexposed controls $P < 0.0001$, Kruskal-Wallis test) (Fig. 1A, B). Similarly, both
218 exposed *fcd-2* and *let-418* mutants accumulated five times more foci than unexposed controls ($P <$
219 0.0001 for both comparisons, Kruskal-Wallis test) (Fig. 1A, B). In *let-418* mutants, the increase was
220 driven by nuclei with multiple foci, sometimes as many as five per nucleus (10.8% of nuclei compared to
221 0.7%). Interestingly, exposed *fcd-2; let-418* double mutants strongly resembled exposed *let-418* single
222 mutants, with over seven times more foci than unexposed controls ($P < 0.0001$, Kruskal-Wallis test) (Fig.
223 1B). Again, this increase was primarily driven by nuclei with multiple foci, especially those with four or
224 five foci (9.6% of nuclei compared to 0.7%). Notably, nuclei with four or five foci were never observed in
225 exposed wild-type or *fcd-2* single mutants. All mutants examined were also more sensitive to cisplatin
226 than wild-type controls. Exposed *fcd-2* single mutants experienced 1.7 times more foci than exposed
227 wild-type populations ($P < 0.0001$), whereas exposed *let-418* single mutants were even more affected,
228 with 2.4 times more foci than exposed wild-type populations ($P < 0.0001$ compared to WT, $P < 0.05$
229 compared to *fcd-2*). The increase in exposed *fcd-2; let-418* double mutants resembled that seen in *let-*
230 *418* single mutants ($P > 0.9$), with the double mutants having 2.7 times more foci than exposed wild-
231 type populations ($P < 0.0001$).
232 We next challenged mutants using hydroxyurea, which stalls replication forks and generates
233 DSBs if left unrepaired (Bailly and Gartner, 2011). A dose of 10 mM was chosen after examining
234 embryonic survival in wild-type and *let-418* mutants across a dose curve (Fig. S3 and Table S6).
235 Hydroxyurea affected all genotypes in a manner similar to cisplatin (Fig. 2 and Table S1). Once again, few
236 DSBs were observed in each unexposed population, with less than 7% of mitotic nuclei containing a
237 RAD-51 focus (Fig. 2A). As expected, exposure to hydroxyurea raised the average number of foci in all
238 genotypes ($P < 0.02$ for all comparisons, Kruskal-Wallis test) (Fig. 2B). Exposed wild-type populations and
239 *fcd-2* mutants had nearly two times more foci than unexposed controls ($P < 0.02$ for both comparisons,
240 Kruskal-Wallis test), both primarily driven by an increase in the number of nuclei with one focus.
241 Resembling what we observed after cisplatin exposure, both single mutants were more sensitive to
242 hydroxyurea than wild-type populations: exposed *fcd-2* single mutants had 1.6 times more foci than
243 exposed wild-type controls ($P < 0.05$) and *let-418* single mutants had twice as many foci as exposed wild-
244 type populations ($P < 0.0001$). As with cisplatin exposure, the response in *fcd-2; let-418* double mutants
245 resembled the response in *let-418* single mutants ($P > 0.9$), with 2.6 times more foci than exposed wild-
246 type populations ($P < 0.0001$). We note that exposed *let-418* and *fcd-2; let-418* mutants each contained
247 nuclei with as many as five RAD-51 foci, which were almost never observed in exposed wild-type or *fcd-*
248 *2* mutant populations (Fig. 2B).

249 To examine whether these unrepaired exogenous DSBs persisted from mitosis into meiosis, we
250 assessed RAD-51 foci throughout pachytene (Fig. 3 and Table S2). Hermaphrodites were exposed to
251 cisplatin or hydroxyurea for twenty hours, allowed to recover for 30-40 hours (to allow mitotic nuclei to
252 progress into mid- or late-pachytene), and dissected for immunofluorescence (Jaramillo-Lambert et al.,
253 2007; Kessler and Yanowitz, 2014). At mid-pachytene, wild-type animals had an average of 3.3 foci per
254 nucleus, which is consistent with prior observations (Fig. 3A, B) (Achache et al., 2021; Cahoon et al.,
255 2023; Colaiácovo et al., 2003; Germoglio et al., 2020; Rosu et al., 2013; Stamper et al., 2013). All
256 unexposed mutants had significantly more RAD-51 foci than unexposed wild-type animals in mid-
257 pachytene ($P < 0.001$ for all mutants, Kruskal-Wallis test; see Table S2 for additional comparisons
258 between early-pachytene and late-pachytene), and the number of foci in *fcd-2; let-418* double mutants
259 resembled that in both single mutants ($P > 0.9$) (Fig. 3A, B).
260 Exposing mitotic nuclei to cisplatin significantly increased the number of foci during mid- or late-
261 pachytene across all genotypes compared to unexposed controls ($P < 0.0001$ for all comparisons) (Fig.
262 3C, D). Notably, all mutants had persistent damage even in late-pachytene (Fig. 3C and Table S2) ($P <$
263 0.05 for all genotypes compared to wild-type) – both *let-418* single mutants and *fcd-2; let-418* double
264 mutants were more affected than *fcd-2* single mutants, with each experiencing an average of over five
265 foci per nucleus in late-pachytene ($P < 0.05$ for each compared to *fcd-2*, $P > 0.9$ for double mutant
266 compared to *let-418*). Similarly, exposure to hydroxyurea significantly increased foci during mid-
267 pachytene in both *let-418* single mutants and *fcd-2; let-418* double mutants compared to unexposed
268 controls ($P < 0.0001$ for both comparisons) (Fig. 3E, F), and this increase persisted into late-pachytene
269 when compared to exposed wild-type animals or *fcd-2* single mutants ($P < 0.0001$ for all comparisons)
270 (Fig. 3E and Table S2).
271 Taken together, these data indicate that cisplatin or hydroxyurea generate mitotic DNA lesions
272 that require both LET-418 and FCD-2 for proper repair. In their absence, exogenous damage incurred
273 during mitosis persists until the end of pachytene. Additionally, when responding to mitotic DNA
274 damage in the germline, *fcd-2; let-418* double mutants phenocopy *let-418* single mutant for both
275 mutagens.
276
277 <u>Unrepaired mitotic DSBs affect oocyte quality in *let-418* mutants.</u>
278 Although *let-418* single mutants accumulate DSBs in the mitotic region and during pachytene,
279 they do not display aneuploidy or chromosome fragmentation, indicating that any remaining DSBs are
280 fully resolved by diakinesis (Turcotte et al., 2018). However, mutants lacking both CHD paralogs, CHD-3

281 and LET-418, suffer from meiotic catastrophe, genome fragmentation, and chromosome fusions
282 (Turcotte et al., 2018), suggesting that NuRD needs at least one CHD component to repair endogenous
283 DSBs. To see whether LET-418 is required for the resolution of exogenous DNA lesions, we exposed
284 hermaphrodites to cisplatin or hydroxyurea for twenty hours and allowed them to recover for sixty
285 hours (Jaramillo-Lambert et al., 2007; Kessler and Yanowitz, 2014). This timing allows us to induce DNA
286 damage in mitotic cells and assess its impact during diakinesis, where we expect to see six DAPI-staining
287 bodies, one for each homologous pair of chromosomes.

288 As expected, unexposed wild-type animals rarely produced aneuploid gametes: when scoring
289 aged mothers in their third day of adulthood, we found that only 9% of oocytes contained five DAPI-
290 stained bivalents (Fig. 4A, C, E, Fig. S2, and Table S3). This result is consistent with previous studies
291 showing that oocyte quality decreases with maternal age (Achache et al., 2021; Andux and Ellis, 2008;
292 Luo et al., 2010; Scharf et al., 2021). Each unexposed mutant produced more aneuploid oocytes than
293 wild-type controls, with at least 16% of nuclei containing fewer than six DAPI bodies ($P < 0.01$ for all
294 comparisons, Fisher's exact test), including oocytes with four DAPI bodies that were never observed in
295 wild-type animals (Fig. 4A, C, E and Fig. S2). We also noted that *let-418* single mutants generated a rare
296 oocyte with seven DAPI bodies (Fig. 4E). The presence of univalents in this nucleus reflected the lack of a
297 chiasmata and failure of crossover formation, which almost never occurs in wild-type animals (Dernburg
298 et al., 1998; Yu et al., 2016). When exposed to 400 µM cisplatin, both *fcd-2* single mutants and *fcd-2; let-*
299 *418* double mutants suffered a significant deterioration in oocyte quality ($P < 0.04$ for both comparisons,
300 Fisher's exact test) (Fig. 4B). Each mutant produced oocytes with more than six DAPI bodies, and *fcd-2;*
301 *let-418* double mutants also produced an oocyte with only three DAPI bodies (Fig. 4F). Although
302 exposure to cisplatin did not induce a statistically significant change in wild-type and *let-418* single
303 mutants ($P > 0.5$ for both comparisons, Fisher's exact test), both genotypes produced oocyte classes that
304 were never observed in unexposed controls (Fig. 4E, F and Table S3).

305 When compared to either single mutant, *fcd-2; let-418* double mutants were more affected by
306 cisplatin exposure ($P < 0.003$ for both comparisons, Fisher's exact test). This difference was driven by
307 oocytes with both more and fewer DAPI bodies: *fcd-2; let-418* double mutants produced more nuclei
308 with four or fewer DAPI bodies, but also nuclei with seven to ten DAPI bodies, indicating a severe
309 disruption in crossover formation (Fig. 4F). Given our findings for mitotic DSBs, where the double
310 mutant phenocopied the *let-418* single mutant (Fig. 1 and Fig. 2), we were surprised to see that
311 diakinesis DAPI body number was significantly more affected in *fcd-2; let-418* double mutants than in
312 *let-418* single mutants. However, both the double mutant and *let-418* single mutant produced the rare

313 category of nuclei with three DAPI bodies (Fig. 4F). The severe reduction in DAPI bodies indicated that at
314 least half of the *C. elegans* genome has experienced chromosomal fusions, a phenotype that was also
315 previously observed in mutants missing both CHD paralogs (Turcotte et al., 2018).
316 Similar to cisplatin, exposure to 10 mM hydroxyurea also induced aneuploidy during diakinesis
317 (Fig. 4C, D and Table S3). Although exposure to hydroxyurea did not cause a statistically significant
318 change in wild-type population or *fcd-2* single mutants ($P > 0.3$ for both comparisons, Fisher's exact
319 test), both genotypes produced oocyte classes that were never observed in unexposed controls (Fig. S2
320 and Table S3). However, unlike what we observed after cisplatin exposure, we did not find that *fcd-2*
321 single mutants produced nuclei with more than six DAPI bodies after hydroxyurea exposure (Fig. 4D),
322 indicating that *fcd-2* mutants were more sensitive to cisplatin. Exposed *let-418* single mutants were
323 significantly affected compared to wild-type controls, producing oocytes with both more than seven and
324 fewer than four DAPI bodies, categories that were never observed in unexposed controls ($P < 0.006$,
325 Fisher's exact test).
326 Challenging *fcd-2; let-418* double mutants with hydroxyurea caused a large deterioration in
327 oocyte quality ($P < 0.009$, Fisher's exact test). Exposed *fcd-2; let-418* double mutants were significantly
328 more affected than either of the exposed single mutant controls ($P < 0.004$ for both comparisons,
329 Fisher's exact test). This decline in oocyte quality was partly driven by nuclei with more than six DAPI
330 bodies (sometimes as many as ten), a category that was only ever observed in exposed *fcd-2; let-418*
331 double mutants and *let-418* single mutants (Fig. S2B and Table S3). Once again, the existence of nuclei
332 with univalents indicates that hydroxyurea also causes a severe failure of crossover formation or
333 chromosome fragmentation (Fig. S2B). Taken together, this assessment of diakinesis nuclei indicates
334 that *fcd-2; let-418* double mutants are more sensitive to interstrand crosslinks and stalled replication
335 forks than either single mutant.
336
337 <u>Mutagen exposure reduces embryonic survival of *let-418* mutants.</u>
338 After having shown that LET-418 is necessary to repair exogenous DSBs during mitosis and
339 meiosis (Fig. 1 through 3) and prevent aneuploidy during diakinesis (Fig. 4), we next examined oocyte
340 viability by assessing embryonic survival (Fig. 5 and Table S4). To capture the impact of mutagen
341 exposure during mitosis, we assessed embryos 60 hours after exposure, which were produced by
342 mothers in their third day of adulthood (Jaramillo-Lambert et al., 2007; Kessler and Yanowitz, 2014). As
343 expected for aged mothers, unexposed wild-type populations had an average embryonic survival of 96%
344 (Fig. 5A). As a positive control for cisplatin sensitivity, we examined *xpf-1 (tm2842)* mutants, which lack

345 an endonuclease involved in the DNA damage response (Ward et al., 2007). Unexposed *xpf-1* mutants
346 have a lower average survival than unexposed wild-type populations ($P < 0.007$, ANOVA) (Fig. 5A), which
347 is reduced even further by cisplatin in a dose-dependent manner (Fig. S1B and Table S6) (Meier et al.,
348 2014; Ward et al., 2007). Survival in unexposed *fcd-2*, *let-418*, or *fcd-2; let-418* mutants did not
349 significantly differ from wild-type populations ($P > 0.1$ for all comparisons), although each mutant
350 displayed more variability and lower averages across replicates compared to wild-type: across both
351 cisplatin and hydroxyurea experiments, *fcd-2* single mutants averaged 86% survival, *let-418* single
352 mutants averaged 77% survival, and *fcd-2; let-418* double mutants averaged 75% survival (Table S4).
353 When challenged with 400 µM cisplatin, embryonic survival in wild-type populations was significantly
354 reduced to 73% ($P < 0.04$). As expected for a positive control, cisplatin exposure reduced *xpf-1* mutant
355 survival more severely than in wild-type populations, down to 39% survival ($P < 0.01$) (Fig. 5A).
356 Embryonic survival in exposed *fcd-2* single mutants was not significantly affected compared to
357 unexposed controls ($P > 0.8$, ANOVA) (Fig. 5A). Conversely, exposed *let-418* single mutants experienced
358 a significant decline in survival, down to 39% ($P < 0.0001$), a decrease 2.4 times more than wild-type and
359 similar to *xpf-1* mutants (Fig. 5A). We noted that cisplatin had a variable impact on *let-418* mutant
360 survival, across both technical and biological replicates. This observation was consistent with previous
361 variability observed in *let-418* mutants (Turcotte et al., 2018): some replicates were completely
362 unaffected, resembling unexposed controls, whereas others suffered complete embryonic lethality that
363 was never observed in wild-type or *xpf-1* positive controls. Again, the effects of cisplatin on embryonic
364 survival in *fcd-2; let-418* double mutants strongly resembled *let-418* single mutants (Fig. 5A). Exposed
365 *fcd-2; let-418* double mutants experienced a significant drop in survival down to 33% ($P < 0.0001$). As
366 seen in *let-418* single mutants, this reduction was 2.7 times more than wild-type and similar to *xpf-1*
367 positive controls. However, in one departure from *let-418* single mutants, we found that cisplatin caused
368 less variability in *fcd-2; let-418* double mutant survival, which had a distribution that overlapped only the
369 lower half of that observed in *let-418* single mutants (Fig. 5A).
370 We next challenged hermaphrodites with 10 mM hydroxyurea to assess the impact on
371 embryonic survival (Fig. 5B). As expected, this low dose of exposure did not significantly reduce survival
372 in wild-type populations or *fcd-2* single mutants ($P > 0.09$ for both comparisons, ANOVA) (Kim et al.,
373 2018). However, *let-418* single mutants were sensitive to hydroxyurea – embryonic survival dropped
374 from 76% in unexposed controls to 46% after exposure ($P < 0.0003$), a reduction 2.1 times more than
375 experienced by wild-type populations (Fig. 5B). Similarly, survival in exposed *fcd-2; let-418* double

376 mutants dropped from 73% down to 36% ($P < 0.0001$), a reduction 2.8 times more than wild-type ($P <$
377 0.0001) (Fig. 5B).
378 Finally, we challenged hermaphrodites with an additional mutagen, nitrogen mustard, which
379 creates both interstrand crosslinks and DNA-protein crosslinks (Fig. S4 and Table S6) (Povirk and Shuker,
380 1994). A low dose of 100 µM did not affect wild-type embryonic survival ($P > 0.9$, ANOVA), whereas a
381 higher dose of 150 µM significantly decreased wild-type survival to 52% ($P < 0.0001$) (Fig. S4). The low
382 100 µM dose of nitrogen mustard decreased survival in both *let-418* and *fcd-2* single mutants ($P <$
383 0.0001 for both comparisons) and the high 150 µM dose further reduced survival to 25% ($P < 0.0001$ for
384 both comparisons, ANOVA). Nitrogen mustard affected *fcd-2; let-418* double mutants similarly to each
385 single mutant ($P > 0.6$ for all comparisons), with survival severely reduced to 10% by the high 150 µM
386 dose ($P < 0.0001$ compared to unexposed control) (Fig. S4). Taken together, the impact of mutagen
387 exposure on embryonic survival indicate that LET-418 is required to resolve exogenous DNA lesions to
388 maintain oocyte viability.
389
390 <u>LET-418's ATPase domain is necessary for its role in germline DSB repair.</u>
391 The protein sequences of *C. elegans* LET-418 and human CHD4 share extensive homology,
392 including three domains: an ATPase domain, a PHD finger domain, and a double chromodomain (Fig. 6A)
393 (Farnung et al., 2020; Käser-Pébernard et al., 2016; Passannante et al., 2010). Computational models of
394 CHD4 structure suggest that each domain has distinct functions: the ATPase domain slides nucleosomes
395 along DNA (Farnung et al., 2020), the PHD finger domains binds specific residues on histone H3 (Farnung
396 et al., 2020; Mansfield et al., 2011) and the chromodomains primarily bind DNA (Bouazoune et al.,
397 2002). Mutations discovered in human patients, along with *in vitro* experiments of CHD4 activity, have
398 implicated each of these domains in CHD4's nucleosome remodeling activity (Farnung et al., 2020;
399 Watson et al., 2012; Weiss et al., 2016), but the impact of each domain has yet to be assessed *in vivo*.
400 Because the kinetics of repair occur rapidly in response to DNA lesions (Kochan et al., 2017; Nair et al.,
401 2017), we hypothesized that LET-418's function in the germline requires its ATPase domain to slide
402 nucleosomes and expose the site of DNA damage.
403 Figures 1 through 5 of this paper relied on the canonical allele *let-418 (n3536)*, a point mutation
404 in the ATPase domain that is hypomorphic, but viable, at the normal husbandry temperature of 20°C
405 (Andersen et al., 2006; Turcotte et al., 2018). We engineered deletion alleles in the *let-418* gene using
406 CRISPR-Cas9 to remove either the PHD finger domain or the ATPase enzymatic domain (see Methods for
407 details). We then assessed the number of embryos produced throughout the entire laying period in each

408 *let-418* mutant (a full brood) under normal husbandry conditions, using the canonical *n3536* allele as a
409 positive control (Fig. 6A and Table S5). Consistent with previous studies, wild-type mothers produced
410 broods that averaged 311 embryos (Fig 6C). Strikingly, mutants that lack the ATPase domain*, syb6818*,
411 were completely sterile and produced no embryos (Fig. 6C). In these ATPase deletion mutants, we also
412 noted a high occurrence of protruding vulvae and a clear body due to absence of germline, which
413 accounts for the complete sterility (Fig. 6B). Conversely, mutants that lack the PHD finger domain,
414 *syb6708*, produced an average brood of 304 embryos, which was not significantly lower than wild-type
415 broods ($P > 0.7$, ANOVA). Consistent with previous reports, average broods of canonical *n3636* mutants
416 were 188 embryos, which represents a significant reduction compared to wild-type broods ($P < 0.001$).
417 We also noted the variability in canonical *n3636* mutant broods: some mothers produced at wild-type
418 levels (~300 embryos), whereas others were completely sterile (McMurchy et al., 2017; Turcotte et al.,
419 2018).
420 Because LET-418 is also involved in development (Erdelyi et al., 2017; Passannante et al., 2010;
421 von Zelewsky et al., 2000), we assessed embryonic survival throughout the full laying period. Average
422 survival of canonical *n3636* mutants was 92%, which represented a slight but significant reduction
423 compared to average wild-type survival of 98% ($P < 0.01$, ANOVA). In *syb6708* PHD deletion mutants,
424 embryonic survival resembled wild-type survival at 99%, similar to what we observed with brood size (P
425 > 0.9) (Fig. 6D). Finally, we were unable to assess survival in *syb6818* ATPase deletion mutants, because
426 all mothers examined were sterile (N = 20). Altogether, our findings support a model in which LET-418's
427 ATPase domain, but not its PHD domain, is necessary for NuRD's role during oogenesis in otherwise
428 wild-type conditions. Future studies will examine whether the PHD domain is necessary for repairing
429 exogenous DNA damage.
430
431 **DISCUSSION**
432 The germline must preserve genome integrity for all future generations, a task that requires
433 extensive coordination between DNA repair machinery and local chromatin environments (Chen and
434 Tyler, 2022; Clouaire and Legube, 2019). At the site of DNA damage, chromatin landscapes help
435 orchestrate repair using either error-prone or error-free DSB repair pathways (Chen and Tyler, 2022).
436 Although the mechanisms of DNA repair have been well-described across species, the role of chromatin
437 remodelers remains poorly understood. In this study, we show that LET-418, the ATPase remodeling
438 subunit of NuRD, is required to maintain oocyte quality when genomes are challenged by exogenous
439 DNA damage. After exposure to cisplatin or hydroxyurea, mutants with reduced LET-418 activity

440 accumulate more DSBs in the germline (Figs. 1-3), generate more aneuploid oocytes (Fig. 4), and suffer
441 from reduced embryonic viability (Fig. 5 and Fig. 6) – phenotypes that strongly resemble those seen in
442 mutants defective for the FA repair pathway (Adamo et al., 2010; Gartner and Engebrecht, 2022; Lee et
443 al., 2010). When testing the genetic relationship between NuRD and the FA pathway, we showed that
444 *let-418* gene activity is epistatic to the FA gene *fcd-2*, which suggests that NuRD nucleosome remodeling
445 is necessary to allow proper functioning of the FA repair pathway.

446 LET-418/CHD4 has been implicated in biological functions that include maintaining repressive
447 chromatin states, repairing DNA damage, and defining cell fate during embryonic development (De Vaux
448 et al., 2013; Guerry et al., 2007; Käser-Pébernard et al., 2016; Kunert et al., 2009; Saudenova and Wicky,
449 2018; Turcotte et al., 2018; Unhavaithaya et al., 2002; von Zelewsky et al., 2000). In mammals, CHD4's
450 role in resisting DNA damage has led to its upregulation in multiple types of cancer: for example, in
451 glioblastoma, CHD4 overexpression is associated with poor prognosis, likely due to its role in promoting
452 DNA damage repair to assure cancer cell survival (Chudnovsky et al., 2014; McKenzie et al., 2019). Other
453 work in ovarian cancer cells, acute myeloid leukemia cells, and mammary cells has shown that depleting
454 CHD4 impairs homologous recombination and sensitizes tumorigenic cells to DNA damaging agents (Pan
455 et al., 2012; Polo et al., 2010; Sperlazza et al., 2015). Similarly, in *C. elegans*, mutations in LET-418 or its
456 paralog CHD3 prevent DSB repair throughout meiotic pachytene, suggesting that LET-418/CHD4's role is
457 highly conserved across taxa (Turcotte et al., 2018).

458 Our work identifies a new role for LET-418/CHD4 in response to genotoxic threats – in the
459 absence of LET-418's ATPase activity, mutants cannot fully repair exogenous DNA damage incurred
460 during mitosis, which ultimately reduces gamete viability and impairs organismal survival. In germlines,
461 LET-418 is associated with other heterochromatin factors that work with small RNA pathways to silence
462 repetitive elements and protect the genome (McMurchy et al., 2017). The DSB repair defects observed
463 in *let-418* mutants may be caused by disruptions in heterochromatin formation or maintenance, leading
464 to higher sensitivity to DNA damaging agents. A similar effect has been observed with the loss of
465 another core component of NuRD, RBBP4 (LIN-53 in *C. elegans*), which sensitizes cells to DNA damaging
466 agents by establishing a permissive chromatin environment and downregulating RAD51 expression
467 (Kitange et al., 2016).

468 We propose that LET-418 and NuRD are required during at least two points in gametogenesis: to
469 repair exogenous damage accumulated in mitosis and to resolve endogenous DSBs formed during
470 meiosis (this study and Turcotte et al., 2018). In the absence of LET-418 or NuRD activity, mitotic
471 damage persists as nuclei enter meiosis, contributing to the increase of DSBs observed in pachytene

472 (this study and Turcotte et al., 2018). The accumulated damage persists until the end of pachytene, and
473 is reflected in aberrant diakinesis oocytes. The increase in meiotic DSBs may be caused by an inability of
474 the FA pathway to access the damage. During meiosis, the FA pathway continues to repair DNA damage
475 caused by replication fork stalling or interstrand crosslinks – after the lesion is recognized, FA
476 component FANCD2 is mono-ubiquitinated and recruited to the lesion, where it mediates a conversion
477 to DSBs and repair by homologous recombination (Ceccaldi et al., 2016; Niraj et al., 2019). Therefore,
478 the loss of LET-418 or NuRD activity may interfere with recognition of the lesion or with recruiting FCD-2
479 to the site of damage.

480 Cytological experiments show that FA components, including FCD-2/FANCD2, are recruited to
481 DNA lesions to mediate repair in the mitotic region of the germline (Collis et al., 2006; Kim et al., 2018;
482 Lee et al., 2010). Our results are consistent with FCD-2 playing a role in resolving mitotic DSBs – when
483 exposed to mutagens, *fcd-2* single mutants generated aneuploid oocytes that were never observed in
484 wild-type populations: some had chromosome fusions, whereas others experienced crossover failure
485 (Fig. 4 and Fig. S2). These defects represent genomic instability that is a consistent hallmark of defects
486 with the FA pathway, and is even used to diagnose human patients for Fanconi anemia (Adamo et al.,
487 2010, 2010; Auerbach, 2009; De Winter and Joenje, 2009; Lee et al., 2007; Rageul and Kim, 2020).
488 However, we were surprised to find that embryonic viability in *fcd-2* mutants was not affected by
489 exposure to either cisplatin or hydroxyurea (Fig. 5), since others have previously reported a cisplatin
490 sensitivity in this mutant background (Adamo et al., 2010; Collis et al., 2006; Germoglio et al., 2020).
491 After examining the timing of exposure and recovery used in those studies, we realized that they
492 primarily assessed how damage induced during late pachytene affected embryonic survival (Jaramillo-
493 Lambert et al., 2007; Kessler and Yanowitz, 2014). In contrast, we used a time course that allowed us to
494 examine the effects of damage induced earlier, during mitosis. Altogether, our results suggest that FCD-
495 2 and the FA pathway are involved in repairing exogenous DSBs, but may not be the sole, or even the
496 main, repair pathway at this point in gametogenesis. However, in the later stages of meiotic prophase,
497 all DSBs must be resolved before chromosome segregation. Therefore, as nuclei approach diplotene,
498 they rely on alternative error-prone DSB repair pathways like NHEJ to resolve remaining DSBs (Macaisne
499 et al., 2018; Smolikov et al., 2007). These pathways usually result in non-crossovers and disruption of
500 chiasmata formation, or can generate chromosome translocations or fusions (Gartner and Engebrecht,
501 2022); we observed both outcomes in diakinesis nuclei of *let-418* mutants.

502 We have also demonstrated that LET-418's activity is epistatic to that of FCD-2 and the FA
503 pathway – the *fcd-2; let-418* double mutant phenocopies the *let-418* single mutant when challenged by

504 exogenous DNA damage in its repair of DSBs and embryonic survival (Fig. 1-3, and Fig. 5). When
505 examining how mitotic DNA lesions affect diakinesis DAPI body formation, we observed that *fcd-2; let-*
506 *418* double mutants were more severely affected by cisplatin and hydroxyurea than either single mutant
507 (Fig. 4 and Fig. S2). Strikingly, double mutant germlines contained classes of diakinesis nuclei that were
508 only seen in one or the other single mutant, suggesting an additive effect of losing both LET-418 and
509 FCD-2 activity. This result indicates that the FA pathway and NuRD may function in separate DSB repair
510 pathways. The use of distinct pathways may be influenced by the region of the germline in which
511 damage was incurred – in addition to the exogenous damage in mitosis caused by mutagen exposure,
512 *let-418* mutants also accumulate damage endogenous DSBs during pachytene, which are not further
513 exacerbated by the loss of FCD-2 in unexposed double mutants (Fig. 4A, C) (Turcotte et al., 2018).
514 *C. elegans* LET-418 shares extensive homology with human CHD4, including an ATPase domain, a
515 PHD finger domain, and a double chromodomain (Käser-Pébernard et al., 2016; Passannante et al.,
516 2010). Computational models indicate that the ATPase domain repositions nucleosomes by sliding them
517 along DNA (Farnung et al., 2020). When examining human patient mutations identified in cancer or the
518 neurodevelopmental disorder Sifrim-Hitz-Weiss syndrome, we noticed that many missense mutations
519 occurred in the ATPase domain, indicating its importance for LET-418 and NuRD function. (Farnung et
520 al., 2020). To test the requirement for LET-418's ATPase activity *in vivo*, we engineered an endogenous
521 deletion of the ATPase domain (allele *syb6818*) and demonstrated that it is essential for LET-418's
522 function in the germline. ATPase deletion mutants were completely sterile, and all homozygote mutants
523 had defective vulvas (Fig. 6). Conversely, deletion of the PHD domain did not affect fertility or embryonic
524 survival, indicating that this domain is dispensable for LET-418's role in the germline in the absence of
525 exogenous DNA damage. Our findings are consistent with deletion of the PHD domain in other contexts.
526 In biochemical assays using recombinant human CHD4, deletion of the PHD domain causes a minor
527 decrease in remodeling, but we note that this study used unmodified histones (Watson et al., 2012). In
528 *Drosophila*, a hypomorphic point mutation to the PHD domain also slightly reduced remodeling ability,
529 but did not otherwise affect binding of Mi2/CHD4 to chromatin (Kovač et al., 2018).
530 The ATPase deletion phenotypes resemble those of *let-418* genetic null alleles, which were
531 previously used to characterize LET-418's role in vulval development (Guerry et al., 2007; von Zelewsky
532 et al., 2000). In somatic tissues, LET-418 belongs to two distinct complexes that have a conserved role in
533 maintaining cell identity – in addition to NuRD, it is also found in MEC, which consists of LET-418, the
534 histone deacetylase HDA-1, and the Krüppel-like protein MEP-1 (Hou et al., 2020; Käser-Pébernard et
535 al., 2016; Pfefferli et al., 2014; Unhavaithaya et al., 2002). As part of these complexes, LET-418 has roles

536 in specifying vulval fate, embryonic and larval development, and defining lifespan (De Vaux et al., 2013;
537 Erdelyi et al., 2017; Guerry et al., 2007; Käser-Pébernard et al., 2014; Passannante et al., 2010;
538 Saudenova and Wicky, 2018; von Zelewsky et al., 2000). Further characterization of these deletion
539 strains will establish their impact after exposure to DNA damaging agents in in roles outside of the
540 germline.

541 Based on our results, we propose the following model. When replication forks are blocked or
542 stalled, NuRD's remodeling activity creates a permissive chromatin environment that allows for the
543 recruitment of FA pathway components, like FCD-2, to repair the damage via homologous
544 recombination. In the absence of NuRD-mediated remodeling, the FA pathway is unable to repair DNA
545 lesions, causing the accumulation of mitotic and meiotic DSBs and their eventual resolution by error-
546 prone pathways later in meiosis. However, it is not clear from our findings whether NuRD functions
547 entirely upstream of the full FA pathway, or whether it mediates an intermediate step during interstrand
548 crosslink repair. For example, it is possible that DNA lesions are first recognized by the FA component
549 FNCM-1 (which acts upstream of FCD-2), which then recruits NuRD to the site of damage. In summary,
550 we've shown that LET-418's nucleosome remodeling activity is necessary to resolve germline DSBs by
551 error-free pathways like the FA pathway. This work highlights the important role of local chromatin
552 landscapes in coordinating DNA damage repair pathways during gametogenesis.
553

554 **DATA AVAILIBILITY**

555 Strains are available from the *Caenorhabditis* Genetics Center or upon request. The authors affirm that
556 all data necessary for confirming the conclusions of the article are present within the article, figures, and
557 tables.
558

559 **ACKNOWLEDGEMENTS**

560 We thank Diana Libuda and Monica Colaiacovo for generously sharing reagents, Cori Cahoon for
561 immunofluorescence advice, and WormBase for gene and sequence information (Davis et al., 2022). We
562 also thank two anonymous reviewers for suggestions that strengthened the manuscript. Strains were
563 provided by the *Caenorhabditis* Genetics Center, which is funded by the National Institutes of Health
564 (NIH) through the Office of Research Infrastructure Programs (P40 OD010440).
565

566 **FUNDING**

D. A. was supported by a UMass Lowell KCS Science Scholarship. T. B. and K. F. were supported by fellowships from the UMass Lowell River Hawk Scholars Academy. K. F. was supported by the Urban Massachusetts LSAMP program, which is funded by the National Science Foundation (EES 2308724). T.B. was supported by the Society for Developmental Biology through a Choose Development! fellowship, which is funded by the National Institutes of Health (R25HD105600). This work was supported by the National Institutes of Health, with grants R15GM117479 and R15HD104115 to P.M.C. and grant R15GM144861 to T.W.L.

CONFLICT OF INTEREST

The authors declare no conflicts of interest.

REFERENCES

Achache, H., Falk, R., Lerner, N., Beatus, T., Tzur, Y.B., 2021. Oocyte aging is controlled by mitogen-activated protein kinase signaling. Aging Cell 20, e13386. https://doi.org/10.1111/acel.13386

Adamo, A., Collis, S.J., Adelman, C.A., Silva, N., Horejsi, Z., Ward, J.D., Martinez-Perez, E., Boulton, S.J., La Volpe, A., 2010. Preventing Nonhomologous End Joining Suppresses DNA Repair Defects of Fanconi Anemia. Molecular Cell 39, 25–35. https://doi.org/10.1016/j.molcel.2010.06.026

Allis, C.D., Jenuwein, T., 2016. The molecular hallmarks of epigenetic control. Nat Rev Genet 17, 487–500. https://doi.org/10.1038/nrg.2016.59

Alpi, A., Pasierbek, P., Gartner, A., Loidl, J., 2003. Genetic and cytological characterization of the recombination protein RAD-51 in *Caenorhabditis elegans*. Chromosoma 112, 6–16. https://doi.org/10.1007/s00412-003-0237-5

Ananthaswamy, D., Croft, J.C., Woozencroft, N., Lee, T.W., 2022. *C. elegans* Gonad Dissection and Freeze Crack for Immunofluorescence and DAPI Staining. JoVE 64204. https://doi.org/10.3791/64204

Andersen, E.C., Lu, X., Horvitz, H.R., 2006. *C. elegans* ISWI and NURF301 antagonize an Rb-like pathway in the determination of multiple cell fates. Development 133, 2695–2704. https://doi.org/10.1242/dev.02444

Andux, S., Ellis, R.E., 2008. Apoptosis Maintains Oocyte Quality in Aging *Caenorhabditis elegans* Females. PLoS Genet 4, e1000295. https://doi.org/10.1371/journal.pgen.1000295

Auerbach, A.D., 2009. Fanconi anemia and its diagnosis. Mutation Research/Fundamental and Molecular Mechanisms of Mutagenesis 668, 4–10. https://doi.org/10.1016/j.mrfmmm.2009.01.013

Auerbach, A.D., 1993. Fanconi anemia diagnosis and the diepoxybutane (DEB) test. Exp Hematol 21, 731–733.

Bailly, A., Gartner, A., 2011. *Caenorhabditis elegans* Radiation Responses, in: DeWeese, T.L., Laiho, M. (Eds.), Molecular Determinants of Radiation Response. Springer New York, New York, NY, pp. 101–123. https://doi.org/10.1007/978-1-4419-8044-1_5

607 Basta, J., Rauchman, M., 2015. The nucleosome remodeling and deacetylase complex in
608 development and disease. Translational Research 165, 36–47.
609 https://doi.org/10.1016/j.trsl.2014.05.003
610 Becker, P.B., Workman, J.L., 2013. Nucleosome Remodeling and Epigenetics. Cold Spring Harbor
611 Perspectives in Biology 5, a017905–a017905.
612 https://doi.org/10.1101/cshperspect.a017905
613 Bouazoune, K., Mitterweger, A., Längst, G., Imhof, A., Akhtar, A., Becker, P.B., 2002. The dMi-2
614 chromodomains are DNA binding modules important for ATP-dependent nucleosome
615 mobilization. The EMBO Journal 21, 2430–2440.
616 https://doi.org/10.1093/emboj/21.10.2430
617 Brenner, S., 1974. THE GENETICS OF *CAENORHABDITIS ELEGANS*. Genetics 77, 71–94.
618 https://doi.org/10.1093/genetics/77.1.71
619 Cahoon, C.K., Richter, C.M., Dayton, A.E., Libuda, D.E., 2023. Sexual dimorphic regulation of
620 recombination by the synaptonemal complex in *C. elegans*. eLife 12, e84538.
621 https://doi.org/10.7554/eLife.84538
622 Ceccaldi, R., Rondinelli, B., D'Andrea, A.D., 2016. Repair Pathway Choices and Consequences at
623 the Double-Strand Break. Trends in Cell Biology 26, 52–64.
624 https://doi.org/10.1016/j.tcb.2015.07.009
625 Chapman, J.R., Taylor, M.R.G., Boulton, S.J., 2012. Playing the End Game: DNA Double-Strand
626 Break Repair Pathway Choice. Molecular Cell 47, 497–510.
627 https://doi.org/10.1016/j.molcel.2012.07.029
628 Chen, Z., Tyler, J.K., 2022. The Chromatin Landscape Channels DNA Double-Strand Breaks to
629 Distinct Repair Pathways. Front. Cell Dev. Biol. 10, 909696.
630 https://doi.org/10.3389/fcell.2022.909696
631 Chudnovsky, Y., Kim, D., Zheng, S., Whyte, W.A., Bansal, M., Bray, M.-A., Gopal, S., Theisen,
632 M.A., Bilodeau, S., Thiru, P., Muffat, J., Yilmaz, O.H., Mitalipova, M., Woolard, K., Lee, J.,
633 Nishimura, R., Sakata, N., Fine, H.A., Carpenter, A.E., Silver, S.J., Verhaak, R.G.W.,
634 Califano, A., Young, R.A., Ligon, K.L., Mellinghoff, I.K., Root, D.E., Sabatini, D.M., Hahn,
635 W.C., Chheda, M.G., 2014. ZFHX4 Interacts with the NuRD Core Member CHD4 and
636 Regulates the Glioblastoma Tumor-Initiating Cell State. Cell Reports 6, 313–324.
637 https://doi.org/10.1016/j.celrep.2013.12.032
638 Clouaire, T., Legube, G., 2019. A Snapshot on the Cis Chromatin Response to DNA Double-
639 Strand Breaks. Trends in Genetics 35, 330–345.
640 https://doi.org/10.1016/j.tig.2019.02.003
641 Colaiácovo, M.P., MacQueen, A.J., Martinez-Perez, E., McDonald, K., Adamo, A., La Volpe, A.,
642 Villeneuve, A.M., 2003. Synaptonemal Complex Assembly in *C. elegans* Is Dispensable
643 for Loading Strand-Exchange Proteins but Critical for Proper Completion of
644 Recombination. Developmental Cell 5, 463–474. https://doi.org/10.1016/S1534-
645 5807(03)00232-6
646 Collis, S.J., Barber, L.J., Ward, J.D., Martin, J.S., Boulton, S.J., 2006. *C. elegans* FANCD2 responds
647 to replication stress and functions in interstrand cross-link repair. DNA Repair 5, 1398–
648 1406. https://doi.org/10.1016/j.dnarep.2006.06.010

649 Datta, A., Brosh Jr., R.M., 2019. Holding All the Cards—How Fanconi Anemia Proteins Deal with
650 Replication Stress and Preserve Genomic Stability. Genes 10, 170.
651 https://doi.org/10.3390/genes10020170
652 Davis, P., Zarowiecki, M., Arnaboldi, V., Becerra, A., Cain, S., Chan, J., Chen, W.J., Cho, J., Da
653 Veiga Beltrame, E., Diamantakis, S., Gao, S., Grigoriadis, D., Grove, C.A., Harris, T.W.,
654 Kishore, R., Le, T., Lee, R.Y.N., Luypaert, M., Müller, H.-M., Nakamura, C., Nuin, P.,
655 Paulini, M., Quinton-Tulloch, M., Raciti, D., Rodgers, F.H., Russell, M., Schindelman, G.,
656 Singh, A., Stickland, T., Van Auken, K., Wang, Q., Williams, G., Wright, A.J., Yook, K.,
657 Berriman, M., Howe, K.L., Schedl, T., Stein, L., Sternberg, P.W., 2022. WormBase in
658 2022—data, processes, and tools for analyzing *Caenorhabditis elegans*. Genetics 220,
659 iyac003. https://doi.org/10.1093/genetics/iyac003
660 De Massy, B., 2013. Initiation of Meiotic Recombination: How and Where? Conservation and
661 Specificities Among Eukaryotes. Annu. Rev. Genet. 47, 563–599.
662 https://doi.org/10.1146/annurev-genet-110711-155423
663 De Vaux, V., Pfefferli, C., Passannante, M., Belhaj, K., Von Essen, A., Sprecher, S.G., Müller, F.,
664 Wicky, C., 2013. The *Caenorhabditis elegans* LET-418/ Mi2 plays a conserved role in
665 lifespan regulation. Aging Cell 12, 1012–1020. https://doi.org/10.1111/acel.12129
666 De Winter, J.P., Joenje, H., 2009. The genetic and molecular basis of Fanconi anemia. Mutation
667 Research/Fundamental and Molecular Mechanisms of Mutagenesis 668, 11–19.
668 https://doi.org/10.1016/j.mrfmmm.2008.11.004
669 Erdelyi, P., Wang, X., Suleski, M., Wicky, C., 2017. A Network of Chromatin Factors Is Regulating
670 the Transition to Postembryonic Development in *Caenorhabditis elegans*. G3
671 Genes|Genomes|Genetics 7, 343–353. https://doi.org/10.1534/g3.116.037747
672 Farnung, L., Ochmann, M., Cramer, P., 2020. Nucleosome-CHD4 chromatin remodeler structure
673 maps human disease mutations. eLife 9, e56178. https://doi.org/10.7554/eLife.56178
674 Gartner, A., Engebrecht, J., 2022. DNA repair, recombination, and damage signaling. Genetics
675 220, iyab178. https://doi.org/10.1093/genetics/iyab178
676 Germoglio, M., Valenti, A., Gallo, I., Forenza, C., Santonicola, P., Silva, N., Adamo, A., 2020. In
677 vivo analysis of FANCD2 recruitment at meiotic DNA breaks in *Caenorhabditis elegans*.
678 Sci Rep 10, 103. https://doi.org/10.1038/s41598-019-57096-1
679 Guerry, F., Marti, C.-O., Zhang, Y., Moroni, P.S., Jaquiéry, E., Müller, F., 2007. The Mi-2
680 nucleosome-remodeling protein LET-418 is targeted via LIN-1/ETS to the promoter of
681 lin-39/Hox during vulval development in *C. elegans*. Developmental Biology 306, 469–
682 479. https://doi.org/10.1016/j.ydbio.2007.03.026
683 Hou, T., Cao, Z., Zhang, J., Tang, M., Tian, Y., Li, Y., Lu, X., Chen, Y., Wang, Hui, Wei, F.-Z., Wang,
684 L., Yang, Y., Zhao, Y., Wang, Z., Wang, Haiying, Zhu, W.-G., 2020. SIRT6 coordinates with
685 CHD4 to promote chromatin relaxation and DNA repair. Nucleic Acids Res 48, 2982–
686 3000. https://doi.org/10.1093/nar/gkaa006
687 Jaramillo-Lambert, A., Ellefson, M., Villeneuve, A.M., Engebrecht, J., 2007. Differential timing of
688 S phases, X chromosome replication, and meiotic prophase in the *C. elegans* germ line.
689 Developmental Biology 308, 206–221. https://doi.org/10.1016/j.ydbio.2007.05.019
690 Käser-Pébernard, S., Müller, F., Wicky, C., 2014. LET-418/Mi2 and SPR-5/LSD1 Cooperatively
691 Prevent Somatic Reprogramming of *C. elegans* Germline Stem Cells. Stem Cell Reports 2,
692 547–559. https://doi.org/10.1016/j.stemcr.2014.02.007

693 Käser-Pébernard, S., Pfefferli, C., Aschinger, C., Wicky, C., 2016. Fine-tuning of chromatin
694 composition and Polycomb recruitment by two Mi2 homologues during *C. elegans* early
695 embryonic development. Epigenetics & Chromatin 9, 39.
696 https://doi.org/10.1186/s13072-016-0091-3
697 Keeney, S., 2007. Spo11 and the Formation of DNA Double-Strand Breaks in Meiosis, in: Egel, R.,
698 Lankenau, D.-H. (Eds.), Recombination and Meiosis, Genome Dynamics and Stability.
699 Springer Berlin Heidelberg, Berlin, Heidelberg, pp. 81–123.
700 https://doi.org/10.1007/7050_2007_026
701 Kehle, J., 1998. dMi-2, a Hunchback-Interacting Protein That Functions in Polycomb Repression.
702 Science 282, 1897–1900. https://doi.org/10.1126/science.282.5395.1897
703 Kessler, Z., Yanowitz, J., 2014. Methodological considerations for mutagen exposure in *C.*
704 *elegans*. Methods 68, 441–449. https://doi.org/10.1016/j.ymeth.2014.04.011
705 Kim, H.-M., Beese-Sims, S.E., Colaiácovo, M.P., 2018. Fanconi Anemia FANCM/FNCM-1 and
706 FANCD2/FCD-2 Are Required for Maintaining Histone Methylation Levels and Interact
707 with the Histone Demethylase LSD1/SPR-5 in *Caenorhabditis elegans*. Genetics 209,
708 409–423. https://doi.org/10.1534/genetics.118.300823
709 Kim, H.-M., Colaiácovo, M.P., 2015. DNA Damage Sensitivity Assays in *Caenorhabditis elegans*.
710 Bio Protoc 5, e1487.
711 Kim, S., Peterson, S.E., Jasin, M., Keeney, S., 2016. Mechanisms of germ line genome instability.
712 Seminars in Cell & Developmental Biology 54, 177–187.
713 https://doi.org/10.1016/j.semcdb.2016.02.019
714 Kitange, G.J., Mladek, A.C., Schroeder, M.A., Pokorny, J.C., Carlson, B.L., Zhang, Y., Nair, A.A.,
715 Lee, J.-H., Yan, H., Decker, P.A., Zhang, Z., Sarkaria, J.N., 2016. Retinoblastoma Binding
716 Protein 4 Modulates Temozolomide Sensitivity in Glioblastoma by Regulating DNA
717 Repair Proteins. Cell Reports 14, 2587–2598.
718 https://doi.org/10.1016/j.celrep.2016.02.045
719 Kochan, J.A., Desclos, E.C.B., Bosch, R., Meister, L., Vriend, L.E.M., van Attikum, H., Krawczyk,
720 P.M., 2017. Meta-analysis of DNA double-strand break response kinetics. Nucleic Acids
721 Res 45, 12625–12637. https://doi.org/10.1093/nar/gkx1128
722 Kovač, K., Sauer, A., Mačinković, I., Awe, S., Finkernagel, F., Hoffmeister, H., Fuchs, A., Müller,
723 R., Rathke, C., Längst, G., Brehm, A., 2018. Tumour-associated missense mutations in the
724 dMi-2 ATPase alters nucleosome remodelling properties in a mutation-specific manner.
725 Nat Commun 9, 2112. https://doi.org/10.1038/s41467-018-04503-2
726 Kunert, N., Wagner, E., Murawska, M., Klinker, H., Kremmer, E., Brehm, A., 2009. dMec: a novel
727 Mi-2 chromatin remodelling complex involved in transcriptional repression. EMBO J 28,
728 533–544. https://doi.org/10.1038/emboj.2009.3
729 Kurhanewicz, N.A., Dinwiddie, D., Bush, Z.D., Libuda, D.E., 2020. Elevated Temperatures Cause
730 Transposon-Associated DNA Damage in *C. elegans* Spermatocytes. Current Biology 30,
731 5007-5017.e4. https://doi.org/10.1016/j.cub.2020.09.050
732 Lachaud, C., Moreno, A., Marchesi, F., Toth, R., Blow, J.J., Rouse, J., 2016. Ubiquitinated Fancd2
733 recruits Fan1 to stalled replication forks to prevent genome instability. Science 351,
734 846–849. https://doi.org/10.1126/science.aad5634

735 Lee, K.Y., Chung, K.Y., Koo, H.-S., 2010. The involvement of FANCM, FANCI, and checkpoint
736 proteins in the interstrand DNA crosslink repair pathway is conserved in *C. elegans*. DNA
737 Repair 9, 374–382. https://doi.org/10.1016/j.dnarep.2009.12.018
738 Lee, K.Y., Yang, I., Park, J.-E., Baek, O.-R., Chung, K.Y., Koo, H.-S., 2007. Developmental stage-
739 and DNA damage-specific functions of *C. elegans* FANCD2. Biochemical and Biophysical
740 Research Communications 352, 479–485. https://doi.org/10.1016/j.bbrc.2006.11.039
741 Luo, S., Kleemann, G.A., Ashraf, J.M., Shaw, W.M., Murphy, C.T., 2010. TGF-β and Insulin
742 Signaling Regulate Reproductive Aging via Oocyte and Germline Quality Maintenance.
743 Cell 143, 299–312. https://doi.org/10.1016/j.cell.2010.09.013
744 Macaisne, N., Kessler, Z., Yanowitz, J.L., 2018. Meiotic Double-Strand Break Proteins Influence
745 Repair Pathway Utilization. Genetics 210, 843–856.
746 https://doi.org/10.1534/genetics.118.301402
747 Mansfield, R.E., Musselman, C.A., Kwan, A.H., Oliver, S.S., Garske, A.L., Davrazou, F., Denu, J.M.,
748 Kutateladze, T.G., Mackay, J.P., 2011. Plant Homeodomain (PHD) Fingers of CHD4 Are
749 Histone H3-binding Modules with Preference for Unmodified H3K4 and Methylated
750 H3K9. Journal of Biological Chemistry 286, 11779–11791.
751 https://doi.org/10.1074/jbc.M110.208207
752 McKenzie, L.D., LeClair, J.W., Miller, K.N., Strong, A.D., Chan, H.L., Oates, E.L., Ligon, K.L.,
753 Brennan, C.W., Chheda, M.G., 2019. CHD4 regulates the DNA damage response and
754 RAD51 expression in glioblastoma. Sci Rep 9, 4444. https://doi.org/10.1038/s41598-
755 019-40327-w
756 McMurchy, A.N., Stempor, P., Gaarenstroom, T., Wysolmerski, B., Dong, Y., Aussianikava, D.,
757 Appert, A., Huang, N., Kolasinska-Zwierz, P., Sapetschnig, A., Miska, E.A., Ahringer, J.,
758 2017. A team of heterochromatin factors collaborates with small RNA pathways to
759 combat repetitive elements and germline stress. eLife 6, e21666.
760 https://doi.org/10.7554/eLife.21666
761 Meier, B., Cooke, S.L., Weiss, J., Bailly, A.P., Alexandrov, L.B., Marshall, J., Raine, K., Maddison,
762 M., Anderson, E., Stratton, M.R., Gartner, A., Campbell, P.J., 2014. *C. elegans* whole-
763 genome sequencing reveals mutational signatures related to carcinogens and DNA
764 repair deficiency. Genome Res. 24, 1624–1636. https://doi.org/10.1101/gr.175547.114
765 Nair, N., Shoaib, M., Sørensen, C.S., 2017. Chromatin Dynamics in Genome Stability: Roles in
766 Suppressing Endogenous DNA Damage and Facilitating DNA Repair. IJMS 18, 1486.
767 https://doi.org/10.3390/ijms18071486
768 Nakanishi, K., Yang, Y.-G., Pierce, A.J., Taniguchi, T., Digweed, M., D'Andrea, A.D., Wang, Z.-Q.,
769 Jasin, M., 2005. Human Fanconi anemia monoubiquitination pathway promotes
770 homologous DNA repair. Proc. Natl. Acad. Sci. U.S.A. 102, 1110–1115.
771 https://doi.org/10.1073/pnas.0407796102
772 Nalepa, G., Clapp, D.W., 2018. Fanconi anaemia and cancer: an intricate relationship. Nat Rev
773 Cancer 18, 168–185. https://doi.org/10.1038/nrc.2017.116
774 Niraj, J., Färkkilä, A., D'Andrea, A.D., 2019. The Fanconi Anemia Pathway in Cancer. Annu. Rev.
775 Cancer Biol. 3, 457–478. https://doi.org/10.1146/annurev-cancerbio-030617-050422
776 Pan, M.-R., Hsieh, H.-J., Dai, H., Hung, W.-C., Li, K., Peng, G., Lin, S.-Y., 2012. Chromodomain
777 Helicase DNA-binding Protein 4 (CHD4) Regulates Homologous Recombination DNA
778 Repair, and Its Deficiency Sensitizes Cells to Poly(ADP-ribose) Polymerase (PARP)

Inhibitor Treatment. Journal of Biological Chemistry 287, 6764–6772. https://doi.org/10.1074/jbc.M111.287037

Passannante, M., Marti, C.-O., Pfefferli, C., Moroni, P.S., Kaeser-Pebernard, S., Puoti, A., Hunziker, P., Wicky, C., Müller, F., 2010. Different Mi-2 Complexes for Various Developmental Functions in *Caenorhabditis elegans*. PLoS ONE 5, e13681. https://doi.org/10.1371/journal.pone.0013681

Pfefferli, C., Müller, F., Jaźwińska, A., Wicky, C., 2014. Specific NuRD components are required for fin regeneration in zebrafish. BMC Biol 12, 30. https://doi.org/10.1186/1741-7007-12-30

Polo, S.E., Kaidi, A., Baskcomb, L., Galanty, Y., Jackson, S.P., 2010. Regulation of DNA-damage responses and cell-cycle progression by the chromatin remodelling factor CHD4. EMBO J 29, 3130–3139. https://doi.org/10.1038/emboj.2010.188

Povirk, L.F., Shuker, D.E., 1994. DNA damage and mutagenesis induced by nitrogen mustards. Mutat Res 318, 205–226. https://doi.org/10.1016/0165-1110(94)90015-9

Rageul, J., Kim, H., 2020. Fanconi anemia and the underlying causes of genomic instability. Environ and Mol Mutagen 61, 693–708. https://doi.org/10.1002/em.22358

Raghunandan, M., Chaudhury, I., Kelich, S.L., Hanenberg, H., Sobeck, A., 2015. FANCD2, FANCJ and BRCA2 cooperate to promote replication fork recovery independently of the Fanconi Anemia core complex. Cell Cycle 14, 342–353. https://doi.org/10.4161/15384101.2014.987614

Rosu, S., Zawadzki, K.A., Stamper, E.L., Libuda, D.E., Reese, A.L., Dernburg, A.F., Villeneuve, A.M., 2013. The *C. elegans* DSB-2 Protein Reveals a Regulatory Network that Controls Competence for Meiotic DSB Formation and Promotes Crossover Assurance. PLoS Genet 9, e1003674. https://doi.org/10.1371/journal.pgen.1003674

Saudenova, M., Wicky, C., 2018. The Chromatin Remodeler LET-418/Mi2 is Required Cell Non-Autonomously for the Post-Embryonic Development of *Caenorhabditis elegans*. JDB 7, 1. https://doi.org/10.3390/jdb7010001

Sayers, E.W., Bolton, E.E., Brister, J.R., Canese, K., Chan, J., Comeau, D.C., Connor, R., Funk, K., Kelly, C., Kim, S., Madej, T., Marchler-Bauer, A., Lanczycki, C., Lathrop, S., Lu, Z., Thibaud-Nissen, F., Murphy, T., Phan, L., Skripchenko, Y., Tse, T., Wang, J., Williams, R., Trawick, B.W., Pruitt, K.D., Sherry, S.T., 2022. Database resources of the national center for biotechnology information. Nucleic Acids Research 50, D20–D26. https://doi.org/10.1093/nar/gkab1112

Scharf, A., Pohl, F., Egan, B.M., Kocsisova, Z., Kornfeld, K., 2021. Reproductive Aging in *Caenorhabditis elegans*: From Molecules to Ecology. Front. Cell Dev. Biol. 9, 718522. https://doi.org/10.3389/fcell.2021.718522

Schindelin, J., Arganda-Carreras, I., Frise, E., Kaynig, V., Longair, M., Pietzsch, T., Preibisch, S., Rueden, C., Saalfeld, S., Schmid, B., Tinevez, J.-Y., White, D.J., Hartenstein, V., Eliceiri, K., Tomancak, P., Cardona, A., 2012. Fiji: an open-source platform for biological-image analysis. Nat Methods 9, 676–682. https://doi.org/10.1038/nmeth.2019

Schlacher, K., Wu, H., Jasin, M., 2012. A Distinct Replication Fork Protection Pathway Connects Fanconi Anemia Tumor Suppressors to RAD51-BRCA1/2. Cancer Cell 22, 106–116. https://doi.org/10.1016/j.ccr.2012.05.015

822 Smolikov, S., Eizinger, A., Hurlburt, A., Rogers, E., Villeneuve, A.M., Colaiácovo, M.P., 2007.
823 Synapsis-defective mutants reveal a correlation between chromosome conformation
824 and the mode of double-strand break repair during *Caenorhabditis elegans* meiosis.
825 Genetics 176, 2027–2033. https://doi.org/10.1534/genetics.107.076968
826 Sperlazza, J., Rahmani, M., Beckta, J., Aust, M., Hawkins, E., Wang, S.Z., Zu Zhu, S., Podder, S.,
827 Dumur, C., Archer, K., Grant, S., Ginder, G.D., 2015. Depletion of the chromatin
828 remodeler CHD4 sensitizes AML blasts to genotoxic agents and reduces tumor
829 formation. Blood 126, 1462–1472. https://doi.org/10.1182/blood-2015-03-631606
830 Stamper, E.L., Rodenbusch, S.E., Rosu, S., Ahringer, J., Villeneuve, A.M., Dernburg, A.F., 2013.
831 Identification of DSB-1, a Protein Required for Initiation of Meiotic Recombination in
832 *Caenorhabditis elegans*, Illuminates a Crossover Assurance Checkpoint. PLoS Genet 9,
833 e1003679. https://doi.org/10.1371/journal.pgen.1003679
834 Stinson, B.M., Loparo, J.J., 2021. Repair of DNA Double-Strand Breaks by the Nonhomologous
835 End Joining Pathway. Annu. Rev. Biochem. 90, 137–164.
836 https://doi.org/10.1146/annurev-biochem-080320-110356
837 Tischkowitz, M., Ameziane, N., Waisfisz, Q., De Winter, J.P., Harris, R., Taniguchi, T., D'Andrea,
838 A., Hodgson, S.V., Mathew, C.G., Joenje, H., 2003. Bi-allelic silencing of the Fanconi
839 anaemia gene *FANCF* in acute myeloid leukaemia: *Short Report*. British Journal of
840 Haematology 123, 469–471. https://doi.org/10.1046/j.1365-2141.2003.04640.x
841 Tischkowitz, M.D., Morgan, N.V., Grimwade, D., Eddy, C., Ball, S., Vorechovsky, I., Langabeer, S.,
842 Stöger, R., Hodgson, S.V., Mathew, C.G., 2004. Deletion and reduced expression of the
843 Fanconi anemia FANCA gene in sporadic acute myeloid leukemia. Leukemia 18, 420–
844 425. https://doi.org/10.1038/sj.leu.2403280
845 Tong, J.K., Hassig, C.A., Schnitzler, G.R., Kingston, R.E., Schreiber, S.L., 1998. Chromatin
846 deacetylation by an ATP-dependent nucleosome remodelling complex. Nature 395,
847 917–921. https://doi.org/10.1038/27699
848 Tsui, V., Crismani, W., 2019. The Fanconi Anemia Pathway and Fertility. Trends in Genetics 35,
849 199–214. https://doi.org/10.1016/j.tig.2018.12.007
850 Turcotte, C.A., Sloat, S.A., Rigothi, J.A., Rosenkranse, E., Northrup, A.L., Andrews, N.P., Checchi,
851 P.M., 2018. Maintenance of Genome Integrity by Mi2 Homologs CHD-3 and LET-418 in
852 *Caenorhabditis elegans*. Genetics 208, 991–1007.
853 https://doi.org/10.1534/genetics.118.300686
854 Unhavaithaya, Y., Shin, T.H., Miliaras, N., Lee, J., Oyama, T., Mello, C.C., 2002. MEP-1 and a
855 Homolog of the NURD Complex Component Mi-2 Act Together to Maintain Germline-
856 Soma Distinctions in *C. elegans*. Cell 111, 991–1002. https://doi.org/10.1016/S0092-
857 8674(02)01202-3
858 von Zelewsky, T., Palladino, F., Brunschwig, K., Tobler, H., Hajnal, A., Müller, F., Brehm, A., 2000.
859 The *C. elegans* Mi-2 chromatin-remodelling proteins function in vulval cell fate
860 determination. Development 127, 5277–5284. https://doi.org/10.1242/dev.127.24.5277
861 Wade, P.A., Jones, P.L., Vermaak, D., Wolffe, A.P., 1998. A multiple subunit Mi-2 histone
862 deacetylase from Xenopus laevis cofractionates with an associated Snf2 superfamily
863 ATPase. Current Biology 8, 843–848. https://doi.org/10.1016/S0960-9822(98)70328-8
864 Wang, Y., Zhang, H., Chen, Y., Sun, Y., Yang, F., Yu, W., Liang, J., Sun, L., Yang, X., Shi, L., Li, R., Li,
865 Y., Zhang, Y., Li, Q., Yi, X., Shang, Y., 2009. LSD1 Is a Subunit of the NuRD Complex and

866 Targets the Metastasis Programs in Breast Cancer. Cell 138, 660–672.
867 https://doi.org/10.1016/j.cell.2009.05.050
868 Ward, J.D., Barber, L.J., Petalcorin, M.I., Yanowitz, J., Boulton, S.J., 2007. Replication blocking
869 lesions present a unique substrate for homologous recombination. EMBO J 26, 3384–
870 3396. https://doi.org/10.1038/sj.emboj.7601766
871 Watson, A.A., Mahajan, P., Mertens, H.D.T., Deery, M.J., Zhang, Wenchao, Pham, P., Du, X.,
872 Bartke, T., Zhang, Wei, Edlich, C., Berridge, G., Chen, Y., Burgess-Brown, N.A.,
873 Kouzarides, T., Wiechens, N., Owen-Hughes, T., Svergun, D.I., Gileadi, O., Laue, E.D.,
874 2012. The PHD and chromo domains regulate the ATPase activity of the human
875 chromatin remodeler CHD4. J Mol Biol 422, 3–17.
876 https://doi.org/10.1016/j.jmb.2012.04.031
877 Weiss, K., Terhal, P.A., Cohen, L., Bruccoleri, M., Irving, M., Martinez, A.F., Rosenfeld, J.A.,
878 Machol, K., Yang, Y., Liu, P., Walkiewicz, M., Beuten, J., Gomez-Ospina, N., Haude, K.,
879 Fong, C.-T., Enns, G.M., Bernstein, J.A., Fan, J., Gotway, G., Ghorbani, M., DDD Study, van
880 Gassen, K., Monroe, G.R., van Haaften, G., Basel-Vanagaite, L., Yang, X.-J., Campeau,
881 P.M., Muenke, M., 2016. De Novo Mutations in CHD4, an ATP-Dependent Chromatin
882 Remodeler Gene, Cause an Intellectual Disability Syndrome with Distinctive
883 Dysmorphisms. Am J Hum Genet 99, 934–941.
884 https://doi.org/10.1016/j.ajhg.2016.08.001
885 Whyte, W.A., Bilodeau, S., Orlando, D.A., Hoke, H.A., Frampton, G.M., Foster, C.T., Cowley,
886 S.M., Young, R.A., 2012. Enhancer decommissioning by LSD1 during embryonic stem cell
887 differentiation. Nature 482, 221–225. https://doi.org/10.1038/nature10805
888 Wilson, T.E., Grawunder, U., Lieber, M.R., 1997. Yeast DNA ligase IV mediates non-homologous
889 DNA end joining. Nature 388, 495–498. https://doi.org/10.1038/41365
890 Woodage, T., Basrai, M.A., Baxevanis, A.D., Hieter, P., Collins, F.S., 1997. Characterization of the
891 CHD family of proteins. Proc. Natl. Acad. Sci. U.S.A. 94, 11472–11477.
892 https://doi.org/10.1073/pnas.94.21.11472
893 Xue, Y., Wong, J., Moreno, G.T., Young, M.K., Côté, J., Wang, W., 1998. NURD, a Novel Complex
894 with Both ATP-Dependent Chromatin-Remodeling and Histone Deacetylase Activities.
895 Molecular Cell 2, 851–861. https://doi.org/10.1016/S1097-2765(00)80299-3
896 Youds, J.L., Barber, L.J., Boulton, S.J., 2009. *C. elegans*: A model of Fanconi anemia and ICL
897 repair. Mutation Research/Fundamental and Molecular Mechanisms of Mutagenesis
898 668, 103–116. https://doi.org/10.1016/j.mrfmmm.2008.11.007
899
900
901 **FIGURE LEGENDS**
902
903 **Figure 1: *let-418* mutants cannot repair mitotic DSBs when challenged with cisplatin.**
904 **(A, B)** Stacked histograms showing the percentage of nuclei with the indicated number of RAD-51 foci
905 for animals exposed to 0 µM (A) and 400 µM of cisplatin (B). Average number of foci per nucleus is
906 indicated under each genotype. Comparisons between wild-type and mutant populations at the same
907 dose are shown directly under averages for each genotype; other comparisons are indicated by

908 horizontal lines. For all genotypes, exposed populations differed significantly from unexposed controls
909 (not indicated on histogram, $P < 0.0001$ for all comparisons). Each condition includes at least 2000 nuclei
910 analyzed from 15 germlines across three biological replicates. (**C, D**) Representative images of mitotic
911 region nuclei in unexposed (C) and exposed (D) animals, with the distal tip oriented to the left (as
912 indicated by white asterisk). Germlines are stained for RAD-51 (in yellow) and DAPI (in blue). Scale bar
913 represents 2 µm. All statistical analyses were performed using a Kruskal-Wallis test with Dunn's post test
914 (n.s. = not significant, * $P < 0.05$, **** $P < 0.0001$). Summary statistics and data are included in Table S1.
915
916 **Figure 2: *let-418* mutants cannot repair mitotic DSBs when challenged with hydroxyurea.**
917 **(A, B)** Stacked histograms showing the percentage of nuclei with the indicated number of RAD-51 foci
918 for animals exposed to 0 mM (A) and 10 mM of hydroxyrea (B). Average number of foci per nucleus is
919 indicated under each genotype. Comparisons between wild-type and mutant populations at the same
920 dose are shown directly under averages for each genotype; other comparisons are indicated by
921 horizontal lines. For all genotypes, exposed populations differed significantly from unexposed
922 populations (not shown on graph, $P < 0.0001$ for all comparisons). Each condition includes at least 2000
923 nuclei analyzed from 15 germlines across three biological replicates. (**C, D**) Representative images of
924 mitotic region nuclei in unexposed (C) and exposed (D) animals, with the distal tip oriented to the left (as
925 indicated by white asterisk). Germlines are stained for RAD-51 (in yellow) and DAPI (in blue). Scale bar
926 represents 2 µm. All statistical analyses were performed using a Kruskal-Wallis test with Dunn's post test
927 (n.s. = not significant, * $P < 0.05$, ** $P < 0.01$, **** $P < 0.0001$). Summary statistics and data are included
928 in Table S1.
929
930 **Figure 3: Mutagen-induced DNA damage persists throughout pachytene in *let-418* mutants.**
931 **(A, C, E)** Quantification of number of nuclei with the indicated number of RAD-51 foci in unexposed (A),
932 cisplatin-exposed (C), and hydroxyurea-exposed (E) hermaphrodites. Dark line indicates average number
933 of foci for each stage of pachytene: early pachytene (EP), mid-pachytene (MP), and late pachytene (LP).
934 Each stage represents at least 100 nuclei scored from three gonads. Averages for mid-pachytene are
935 shown under each genotype. All comparisons shown are only for mid-pachytene regions (comparisons
936 for early- and late-pachytene regions are included in Table S2): comparison between exposed and
937 unexposed populations are shown under averages; other comparisons are indicated by horizontal lines.
938 **(B, D, F)** Representative immunofluorescence images of mid-pachytene nuclei stained for RAD-51
939 (yellow) and DAPI (blue) in unexposed (B), cisplatin-exposed (D), and hydroxyurea-exposed (F)

940 hermaphrodites. Scale bar represents 2 µm. Summary statistics and data are included in Table S2. All
941 statistical analyses were performed using a Kruskal-Wallis test with Dunn's post test (n.s. = not
942 significant, **** $P < 0.0001$).
943
944 **Figure 4: *let-418* mutants have poor oocyte quality due to mutagen induced mitotic DSBs.**
945 **(A, B, C, D)** Stacked histograms showing the percentage of nuclei with the indicated number of DAPI
946 bodies for animals exposed to 0 µM of cisplatin (A), 400 µM of cisplatin (B), 0 mM of hydroxyurea (C)
947 and 10 mM of hydroxyurea (D). Comparisons between wild-type and mutant populations at the same
948 dose are shown directly under averages for each genotype; other comparisons are indicated by
949 horizontal lines. Each condition includes at least 100 nuclei analyzed from 27 germlines across three
950 biological replicates. **(E, F)** Representative images of -1 oocytes in animals exposed to 0 uM (E) and 400
951 uM of cisplatin (F). See Fig. S2 for representative images of -1 oocytes exposed to hydroxyurea.
952 Germlines are stained with DAPI (in white). Scale bar represents 2 µm. All statistical analyses were
953 performed as a Fisher's exact test on number of DAPI bodies (n.s. = not significant, * $P < 0.05$, ** $P <$
954 0.01, **** $P < 0.0001$). Summary statistics and data are included in Table S3.
955
956 **Figure 5: DNA damaging agents reduce embryonic viability in *let-418* mutants.**
957 (**A, B**) Percent survival of indicated genotypes with and without exposure to cisplatin (A) or hydroxyurea
958 (B); dose is indicated with triangle above genotype names, with cisplatin in salmon (0 µM and 400 µM)
959 and hydroxyurea in blue (0 mM and 10 mM). For all conditions in (A) N=125 and (B) N=150. Dark line
960 represents the mean and whiskers represent S.E.M. Comparisons between wild-type and mutant
961 populations at the same dose are above each condition; other comparisons are indicated by horizontal
962 lines. All statistical analyses were performed using a one-way ANOVA with a Šídák correction (n.s. = not
963 significant, *$P < 0.05$, ** $P < 0.01$, *** $P < 0.001$, **** $P < 0.0001$). Summary statistics and data are
964 found in Table S4.
965
966 **Figure 6: The ATPase motor domain is necessary for LET-418 protein function in DSB repair.**
967 **(A)** Protein alignment of human CHD4 and *C. elegans* LET-418 homologs showing conserved domains.
968 Primary structural alignments were performed according to NCBI-predicted domains using UniProt.
969 Locations of each allele are indicated above the alignment: *syb6708* PHD finger deletion (magenta),
970 canonical *n3536* missense mutation (pink), and *syb6818* ATPase deletion (teal). (**B**) Images of young
971 adult hermaphrodites. The ATPase deletion *syb6818*, has a protruding vulva phenotype (arrow to pVulv)

972 and a lack of germline as indicated by the white space in the body. Scale bar, 100 µm. (**C**) Total brood
973 was assessed in wild-type (gray), *n3536* canonical allele mutants (light pink), *syb6708* PHD finger
974 deletion mutants (magenta), and *syb6818* ATPase deletion mutants (teal). (**D**) Percent embryonic
975 survival, excluding *syb6818* due to complete sterility. For both graphs, dark line represents mean and
976 whiskers represent S.E.M. All statistical analyses were performed using ANOVA with a Šídák correction
977 (n.s. = not significant, *$P < 0.05$, **$P < 0.01$, *** $P < 0.001$, **** $P < 0.0001$). Summary statistics and data
978 are included in Table S5.
979
980 **Figure S1: Cisplatin affects embryonic survival in a dose-dependent manner.**
981 (**A, B**) Mean percent survival of wild-type populations (gray) exposed to doses of cisplatin ranging from 0
982 µM to 700 µM (A) or 0 µM to 400 µM (B). Relative dose levels are indicated by triangles under the X-
983 axis. (B) Examining the effects of cisplatin on *let-418* mutants (pink), with *xpf-1* mutants (green) included
984 as a positive control for cisplatin sensitivity. Whiskers represent S.E.M. For each condition, at least 25
985 broods were evaluated. Summary statistics and data are included in Table S6.
986
987 **Figure S2: *let-418* mutants have poor oocyte quality due to hydroxyurea induced mitotic DSBs.**
988 (**A, B**) Representative images of -1 oocytes in unexposed (A) and exposed (B) animals. Germlines are
989 stained with DAPI (in white). Scale bar represents 2 µm. Summary statistics and data are included in
990 Table S3.
991
992 **Figure S3: Hydroxyurea affects embryonic survival in a dose-dependent manner.**
993 Mean percent survival of wild-type (gray) and *let-418* mutants (pink) exposed to increasing doses of
994 hydroxyurea (from 0 mM to 10 mM, with relative levels indicated by the blue triangle under the X-axis).
995 Whiskers represent S.E.M. For each condition, at least 25 broods were evaluated. Summary statistics
996 and data are included in Table S6.
997
998 **Figure S4: Nitrogen mustard reduces embryonic survival in *let-418* and *fcd-2* mutants.**
999 Percent survival of indicated genotypes with and without exposure nitrogen mustard; brown triangles
1000 indicate dose (0 mM, 100 mM, and 150 mM). Dark line represents mean percent survival and whiskers
1001 represent S.E.M. . Comparisons between wild-type and mutant populations at the same dose are above
1002 each mutant; other comparisons are indicated by horizontal lines. All statistical analyses were

1003 performed using ANOVA followed by Šídák's multiple comparisons (**$P < 0.01$, *** $P < 0.001$, **** $P <$

1004 0.0001). Summary statistics and data are included in Table S6.

FIGURES WITH LEGENDS

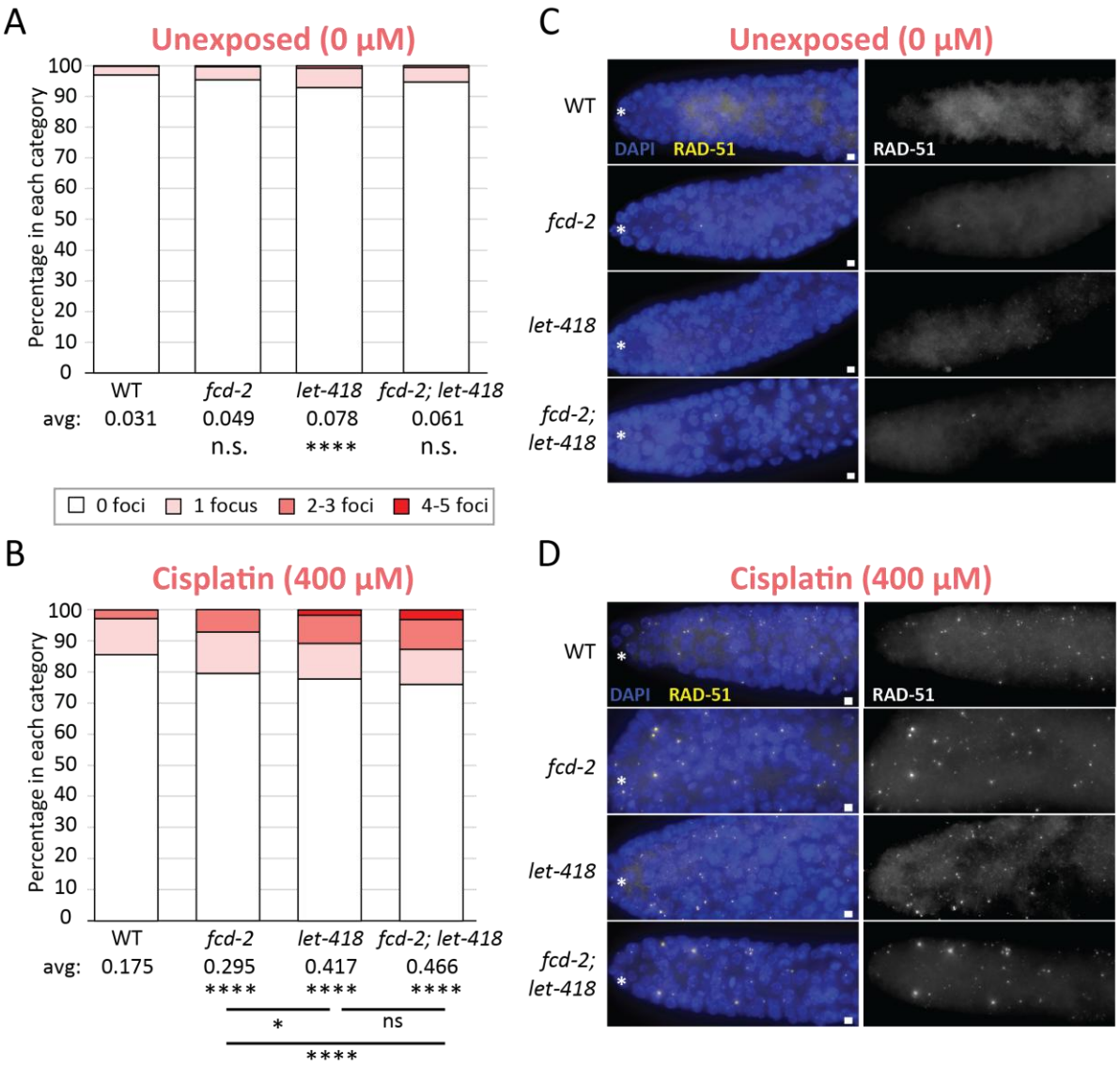

Figure 1: *let-418* mutants cannot repair mitotic DSBs when challenged with cisplatin.
(A, B) Stacked histograms showing the percentage of nuclei with the indicated number of RAD-51 foci for animals exposed to 0 µM (A) and 400 µM of cisplatin (B). Average number of foci per nucleus is indicated under each genotype. Comparisons between wild-type and mutant populations at the same dose are shown directly under averages for each genotype; other comparisons are indicated by horizontal lines. For all genotypes, exposed populations differed significantly from unexposed controls (not indicated on histogram, $P < 0.0001$ for all comparisons). Each condition includes at least 2000 nuclei analyzed from 15 germlines across three biological replicates. (**C, D**) Representative images of mitotic region nuclei in unexposed (C) and exposed (D) animals, with the distal tip oriented to the left (as indicated by white asterisk). Germlines are stained for RAD-51 (in yellow) and DAPI (in blue). Scale bar represents 2 µm. All statistical analyses were performed using a Kruskal-Wallis test with Dunn's post test (n.s. = not significant, * $P < 0.05$, **** $P < 0.0001$). Summary statistics and data are included in Table S1.

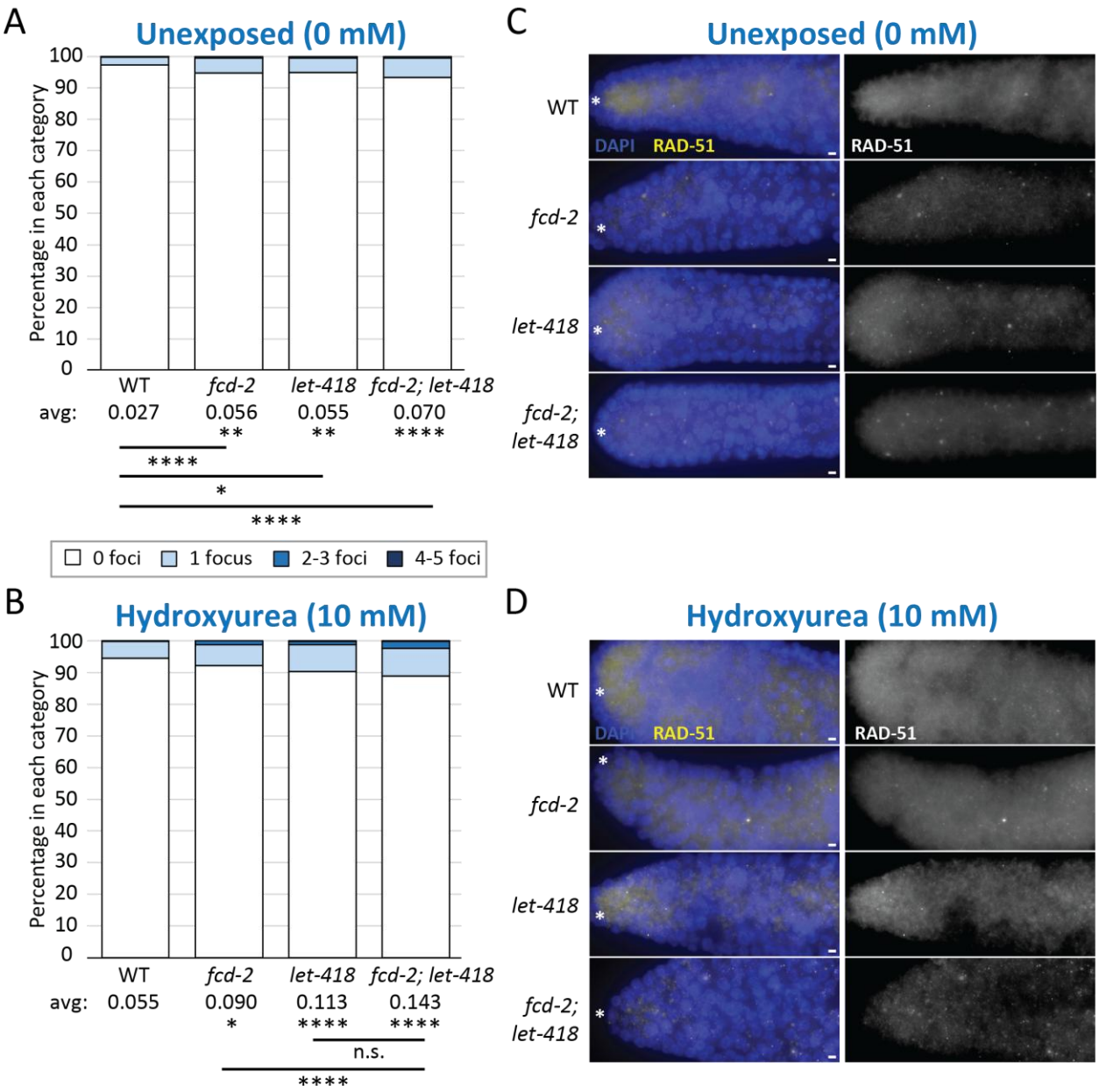

Figure 2: *let-418* mutants cannot repair mitotic DSBs when challenged with hydroxyurea.
(A, B) Stacked histograms showing the percentage of nuclei with the indicated number of RAD-51 foci for animals exposed to 0 mM (A) and 10 mM of hydroxyrea (B). Average number of foci per nucleus is indicated under each genotype. Comparisons between wild-type and mutant populations at the same dose are shown directly under averages for each genotype; other comparisons are indicated by horizontal lines. For all genotypes, exposed populations differed significantly from unexposed populations (not shown on graph, $P < 0.0001$ for all comparisons). Each condition includes at least 2000 nuclei analyzed from 15 germlines across three biological replicates. (**C, D**) Representative images of mitotic region nuclei in unexposed (C) and exposed (D) animals, with the distal tip oriented to the left (as indicated by white asterisk). Germlines are stained for RAD-51 (in yellow) and DAPI (in blue). Scale bar represents 2 µm. All statistical analyses were performed using a Kruskal-Wallis test with Dunn's post test (n.s. = not significant, * $P < 0.05$, ** $P < 0.01$, **** $P < 0.0001$). Summary statistics and data are included in Table S1.

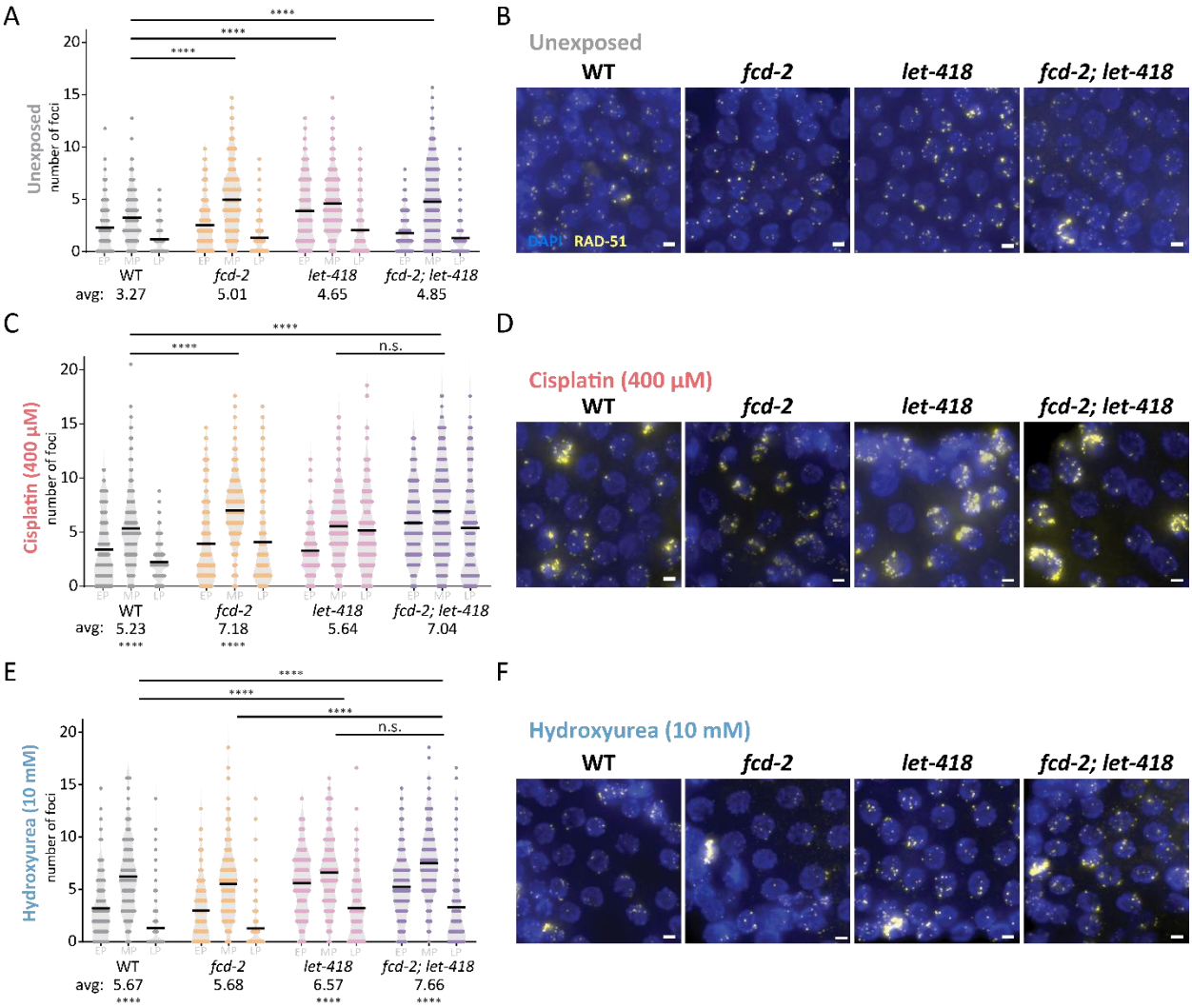

Figure 3: Mutagen-induced DNA damage persists throughout pachytene in *let-418* mutants.
(A, C, E) Quantification of number of nuclei with the indicated number of RAD-51 foci in unexposed (A), cisplatin-exposed (C), and hydroxyurea-exposed (E) hermaphrodites. Dark line indicates average number of foci for each stage of pachytene: early pachytene (EP), mid-pachytene (MP), and late pachytene (LP). Each stage represents at least 100 nuclei scored from three gonads. Averages for mid-pachytene are shown under each genotype. All comparisons shown are only for mid-pachytene regions (comparisons for early- and late-pachytene regions are included in Table S2): comparison between exposed and unexposed populations are shown under averages; other comparisons are indicated by horizontal lines. **(B, D, F)** Representative immunofluorescence images of mid-pachytene nuclei stained for RAD-51 (yellow) and DAPI (blue) in unexposed (B), cisplatin-exposed (D), and hydroxyurea-exposed (F) hermaphrodites. Scale bar represents 2 µm. Summary statistics and data are included in Table S2. All statistical analyses were performed using a Kruskal-Wallis test with Dunn's post test (n.s. = not significant, **** $P < 0.0001$).

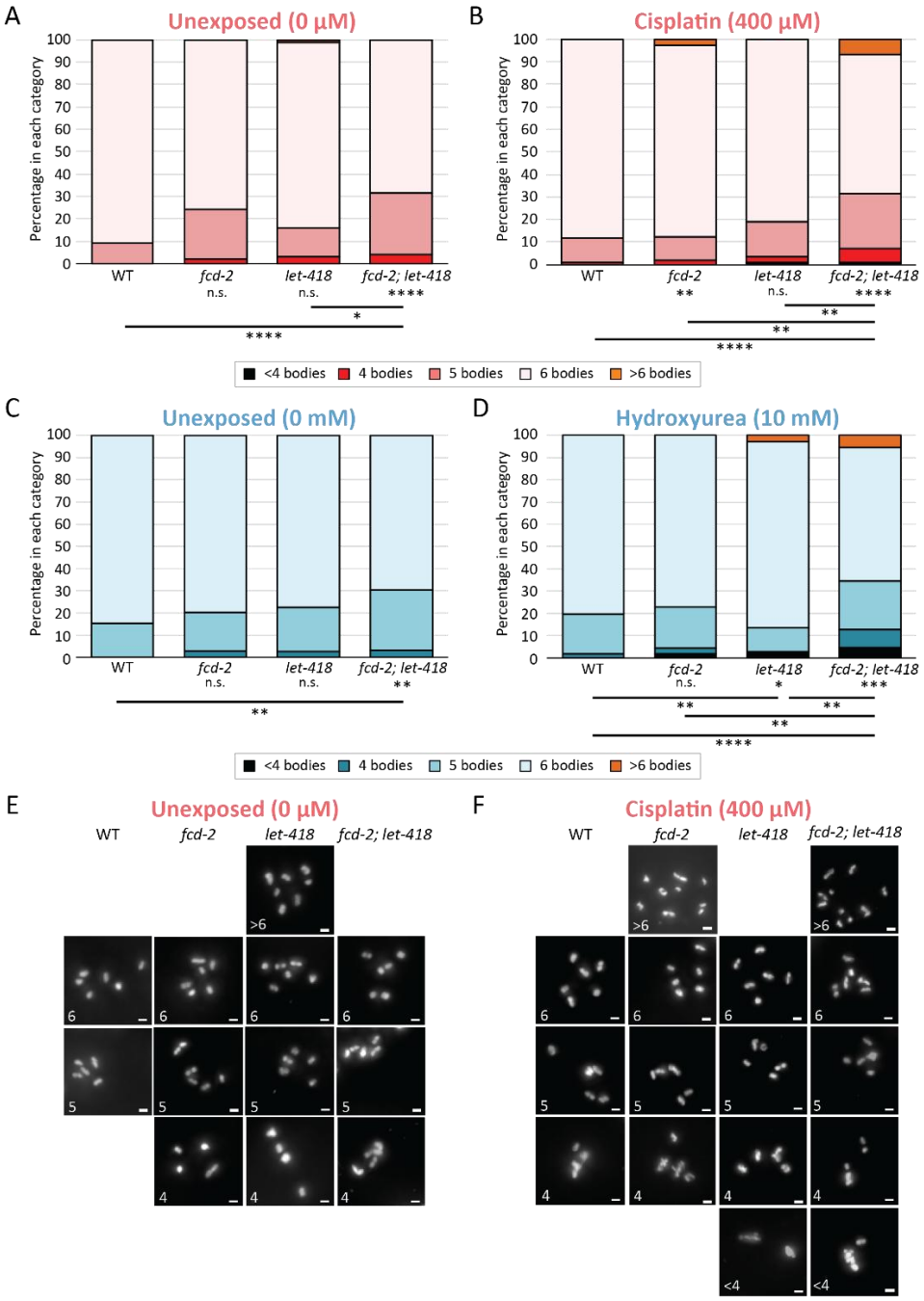

Figure 4: *let-418* mutants have poor oocyte quality due to mutagen induced mitotic DSBs.
(A, B, C, D) Stacked histograms showing the percentage of nuclei with the indicated number of DAPI bodies for animals exposed to 0 µM of cisplatin (A), 400 µM of cisplatin (B), 0 mM of hydroxyurea (C) and 10 mM of hydroxyurea (D). Comparisons between wild-type and mutant populations at the same dose are shown directly under averages for each genotype; other comparisons are indicated by horizontal lines. Each condition includes at least 100 nuclei analyzed from 27 germlines across three biological replicates. **(E, F)** Representative images of -1 oocytes in animals exposed to 0 uM (E) and 400 uM of cisplatin (F). See Fig. S1 for representative images of -1 oocytes exposed to hydroxyurea. Germlines are stained with DAPI (in white). Scale bar represents 2 µm. All statistical analyses were performed as a Fisher's exact test on number of DAPI bodies (n.s. = not significant, * $P < 0.05$, ** $P < 0.01$, **** $P < 0.0001$). Summary statistics and data are included in Table S3.

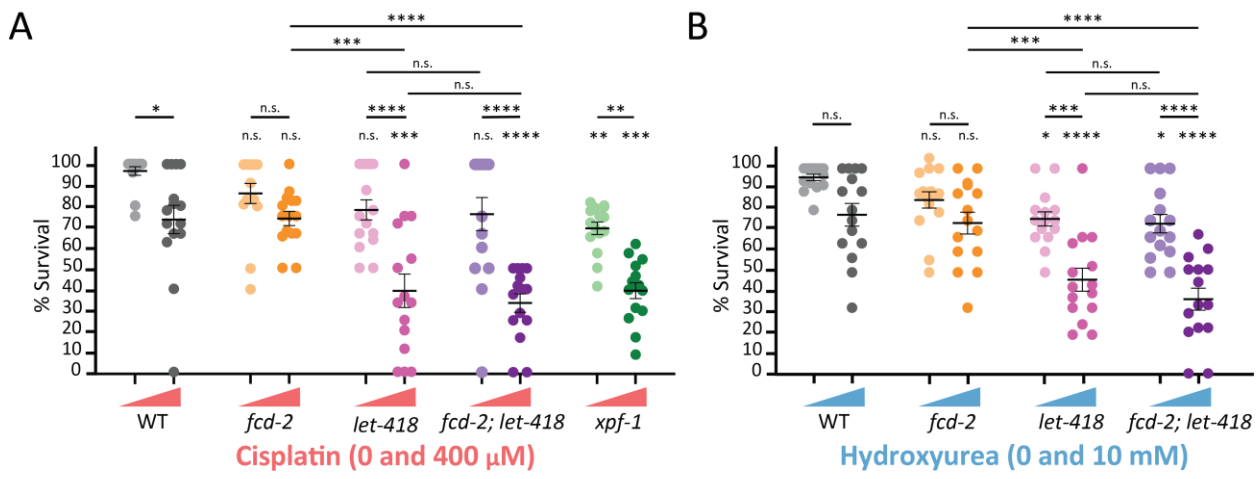

Figure 5: DNA damaging agents reduce embryonic viability in *let-418* mutants.
(**A, B**) Percent survival of indicated genotypes with and without exposure to cisplatin (A) or hydroxyurea (B); dose is indicated with triangle above genotype names, with cisplatin in salmon (0 µM and 400 µM) and hydroxyurea in blue (0 mM and 10 mM). For all conditions in (A) N=125 and (B) N=150. Dark line represents the mean and whiskers represent S.E.M. Comparisons between wild-type and mutant populations at the same dose are above each condition; other comparisons are indicated by horizontal lines. All statistical analyses were performed using a one-way ANOVA with a Šídák correction (n.s. = not significant, *$P < 0.05$, ** $P < 0.01$, *** $P < 0.001$, **** $P < 0.0001$). Summary statistics and data are found in Table S4.

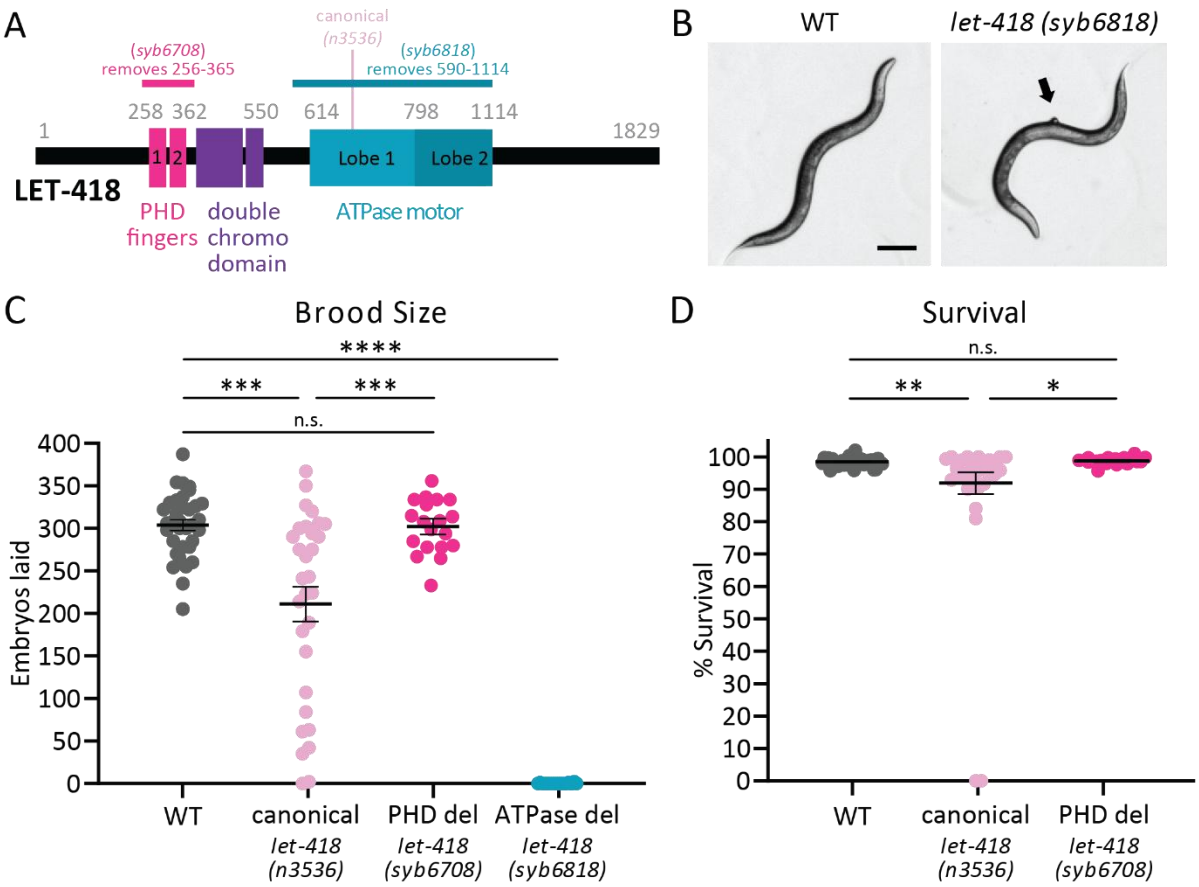

Figure 6: The ATPase motor domain is necessary for LET-418 protein function in DSB repair.
(A) Protein alignment of human CHD4 and *C. elegans* LET-418 homologs showing conserved domains. Primary structural alignments were performed according to NCBI-predicted domains using UniProt. Locations of each allele are indicated above the alignment: *syb6708* PHD finger deletion (magenta), canonical *n3536* missense mutation (pink), and *syb6818* ATPase deletion (teal). (**B**) Images of young adult hermaphrodites. The ATPase deletion *syb6818*, has a protruding vulva phenotype (arrow to pVulv) and a lack of germline as indicated by the white space in the body. Scale bar, 100 µm. (**C**) Total brood was assessed in wild-type (gray), *n3536* canonical allele mutants (light pink), *syb6708* PHD finger deletion mutants (magenta), and *syb6818* ATPase deletion mutants (teal). (**D**) Percent embryonic survival, excluding *syb6818* due to complete sterility. For both graphs, dark line represents mean and whiskers represent S.E.M. All statistical analyses were performed using ANOVA with a Šídák correction (n.s. = not significant, *$P < 0.05$, **$P < 0.01$, *** $P < 0.001$, **** $P < 0.0001$). Summary statistics and data are included in Table S5.

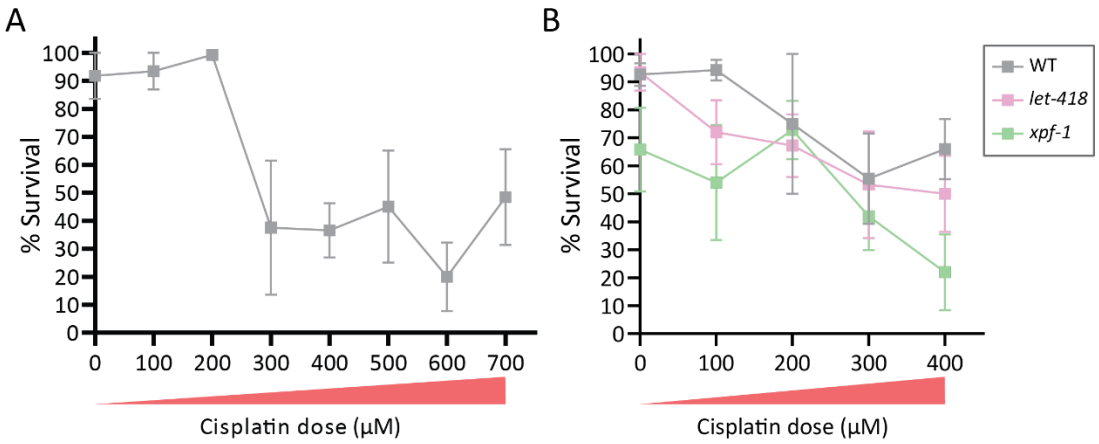

Figure S1: Cisplatin affects embryonic survival in a dose-dependent manner.
(**A, B**) Mean percent survival of wild-type populations (gray) exposed to doses of cisplatin ranging from 0 µM to 700 µM (A) or 0 µM to 400 µM (B). Relative dose levels are indicated by triangles under the X-axis. (B) Examining the effects of cisplatin on *let-418* mutants (pink), with *xpf-1* mutants (green) included as a positive control for cisplatin sensitivity. Whiskers represent S.E.M. For each condition, at least 25 broods were evaluated. Summary statistics and data are included in Table S6.

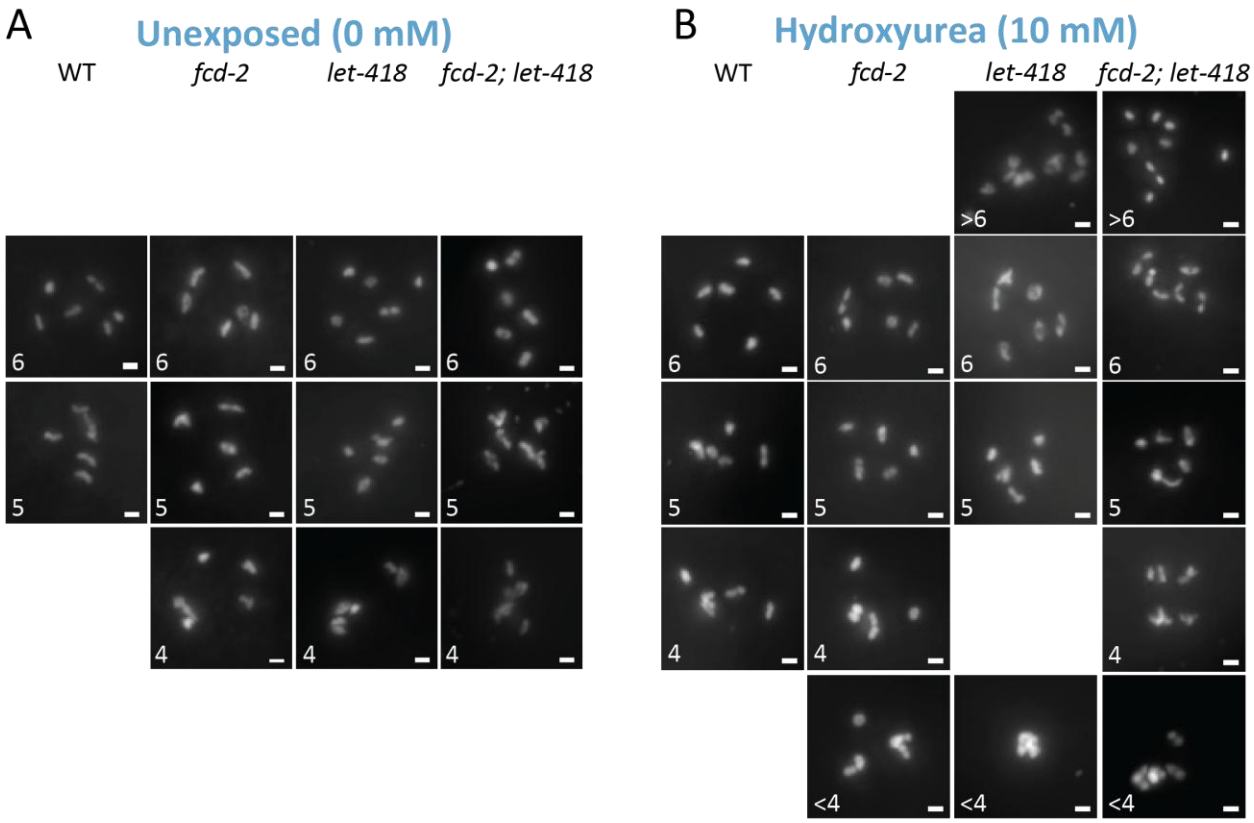

Figure S2: *let-418* mutants have poor oocyte quality due to hydroxyurea induced mitotic DSBs.
(**A, B**) Representative images of -1 oocytes in unexposed (A) and exposed (B) animals. Germlines are stained with DAPI (in white). Scale bar represents 2 µm. Summary statistics and data are included in Table S3.

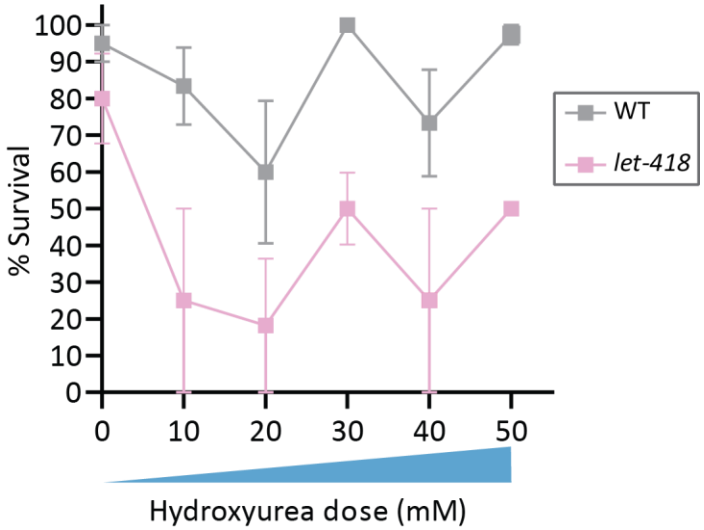

Figure S3: Hydroxyurea affects embryonic survival in a dose-dependent manner.
Mean percent survival of wild-type (gray) and *let-418* mutants (pink) exposed to increasing doses of hydroxyurea (from 0 mM to 10 mM, with relative levels indicated by the blue triangle under the X-axis). Whiskers represent S.E.M. For each condition, at least 25 broods were evaluated. Summary statistics and data are included in Table S6.

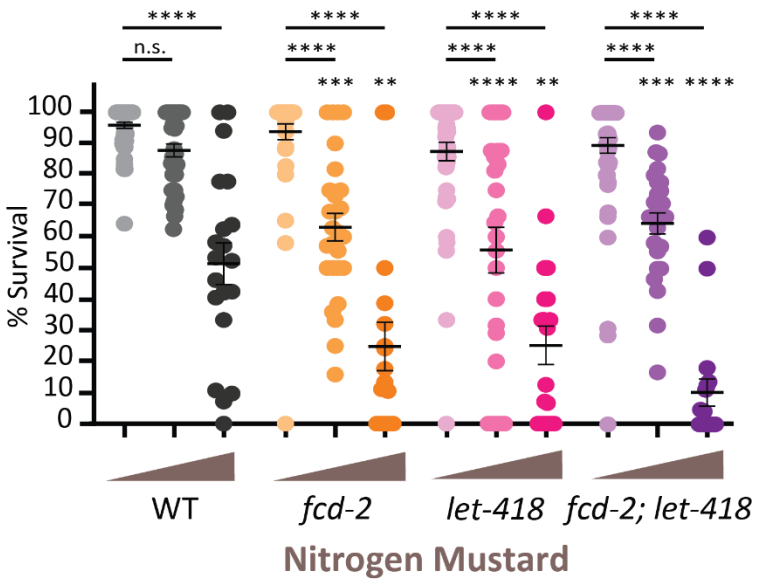

Figure S4: Nitrogen mustard reduces embryonic survival in *let-418* and *fcd-2* mutants.
Percent survival of indicated genotypes with and without exposure nitrogen mustard; brown triangles indicate dose (0 mM, 100 mM, and 150 mM). Dark line represents mean percent survival and whiskers represent S.E.M. . Comparisons between wild-type and mutant populations at the same dose are above each mutant; other comparisons are indicated by horizontal lines. All statistical analyses were performed using ANOVA followed by Šídák's multiple comparisons (**$P < 0.01$, *** $P < 0.001$, **** $P < 0.0001$). Summary statistics and data are included in Table S6.